Journal of Drug Delivery Science and Technology 109 (2025) 107001

Contents lists available at ScienceDirect

Journal of Drug Delivery Science and Technology

journal homepage: www.elsevier.com/locate/jddst

Unraveling the potential of bioadhesive antimicrobial microparticles for the treatment of prosthetic joint infections

F.C. Luciano [a], I. Yuste [a], P. Sanz-Ruiz [b], A. Ribed-Sánchez [c], M.P. Ballesteros [a,g], C. Rodríguez [d], B.J. Anaya [a], M. Tiboni [e], G. Maurizzi [e], L. Casettari [e], E. González-Burgos [f,*], D.R. Serrano [a,g,**]

[a] Pharmaceutics and Food Technology Department, Faculty of Pharmacy, Universidad Complutense de Madrid, Plaza Ramón y Cajal S/n, 28040, Madrid, Spain
[b] Orthopaedic and Trauma Department, Hospital General Universitario, Gregorio Marañón, Doctor Esquerdo 46, 28029, Madrid, Spain
[c] Pharmacy Unit, Hospital General Universitario, Gregorio Marañón, Doctor Esquerdo 46, 28029, Madrid, Spain
[d] Department of Microbiology and Parasitology, Faculty of Pharmacy, Universidad Complutense de Madrid (UCM), Madrid, Spain
[e] Department of Biomolecular Sciences, University of Urbino Carlo Bo, Piazza Del Rinascimento, 6, 61029, Urbino, PU, Italy
[f] Department of Pharmacology, Pharmacognosy and Botany, Faculty of Pharmacy, Universidad Complutense de Madrid (UCM), Madrid, Spain
[g] Instituto Universitario de Farmacia Industrial, Faculty of Pharmacy, Universidad Complutense de Madrid, 28040, Madrid, Spain

ARTICLE INFO

Keywords:
Microparticles
Amphotericin B
Vancomycin
Periprosthetic joint infections
Prosthesis

ABSTRACT

Periprosthetic joint infections (PJIs) are serious complications following hip or knee arthroplasty, and current preventive and therapeutic strategies remain suboptimal due to inadequate antimicrobial efficacy. This study explores a novel approach for preventing and treating bacterial and fungal PJIs using smart bioadhesive microparticles obtained by spray drying and loaded with vancomycin (a broad-spectrum antibacterial) and amphotericin B (AmB, an antifungal). Dry microparticles were redispersed into a hyaluronic gel before adhesion to the prosthesis. The microparticles exhibited a sustained drug release profile, characterized by an initial burst release (40 %–80 % for AmB and vancomycin respectively) within the first 10 h, followed by prolonged release over seven days. The formulation demonstrated high efficacy against multiple pathogens, including *Staphylococcus* spp. (*S. epidermidis* and *S. aureus*) and *Candida* spp. (*C. albicans, C. parapsilopsis, C. glabrata,* and *C. krusei*). Additionally, the microparticles showed low hemolytic toxicity and provided a protective effect on mammalian cell lines (Saos-2, BJ, hFOB). These findings highlight a promising strategy for PJI prophylaxis and treatment, with potential for seamless integration into clinical practice.

1. Introduction

Periprosthetic joint infections (PJIs) are significant complications following joint arthroplasty, characterized by complex diagnostic and treatment challenges. These infections can lead to severe patient morbidity and increased healthcare costs. The diagnosis and management of PJIs are complicated by their heterogeneous clinical presentations and the lack of a universally accepted diagnostic standard [1,2].

PJIs often require long and complex treatments, representing high morbidity associated with implant removal and even death. Most surgical infections associated with arthroplasties have their origin at the time of surgery because of the bacterial flora of the patient's skin, which is difficult to fully eradicate with conventional antiseptics. The suppression status due to surgery and the easier bacterial colonization due to the use of metal implants. Moreover, infections can also occur later by the hematogenous route [3,4]. More than two-thirds of PJIs are caused by intraoperative microorganisms [5]. Bacterial PJIs have a higher incidence compared to fungal ones (10 % *vs* 1 % of the cases) [6,7]. The major bacteria responsible for PJIs are Gram-positive bacteria such as *Staphylococcus aureus* and *S. epidermidis* in 70 % of all cases [8]. However, Gram-negative bacteria, such as *Pseudomonas aeruginosa* can also occur, in less percentage, but cause devastating problems [9,10].

Fungal PJIs are a rare but severe complication following joint

* Corresponding author.
** Corresponding author. Pharmaceutics and Food Technology Department, Faculty of Pharmacy, Universidad Complutense de Madrid, Plaza Ramón y Cajal S/n, 28040, Madrid, Spain.
E-mail addresses: elenagon@ucm.es (E. González-Burgos), drserran@ucm.es (D.R. Serrano).

https://doi.org/10.1016/j.jddst.2025.107001
Received 26 September 2024; Received in revised form 1 May 2025; Accepted 2 May 2025
Available online 6 May 2025

arthroplasty, primarily caused by *Candida species*. *Candida albicans* is the predominant species, followed by *C. parapsilosis*, *C. glabrata, and C. tropicalis* [11]. These infections pose significant diagnostic and therapeutic challenges due to their complex nature and the lack of standardized treatment protocols. The management of fungal PJIs often involves a combination of surgical intervention and antifungal therapy, with varying success rates depending on the approach used [12,13].

Polymicrobial PJIs present a significant clinical challenge, particularly when involving both bacterial and fungal pathogens. These infections are complex due to the diverse microbial interactions and the difficulty in achieving successful treatment outcomes. The prevalence of co-infections involving fungal pathogens, such as *Candida species*, is notable, with studies indicating that up to 15 % of PJIs may involve both bacterial and fungal organisms [14,15]. Fungal PJIs, although less common than bacterial PJIs, are increasingly recognized, with *Candida species* being the most prevalent fungal pathogens. In a study of 269 patients with Candida PJI, 51.3 % had co-infections with bacteria, highlighting the polymicrobial nature of these infections [16,17]. The presence of fungal pathogens alongside bacteria can exacerbate the infection and complicate treatment strategies.

Polymicrobial infections involving *Candida* and *S. aureus* are associated with higher mortality rates compared to monomicrobial infections. For instance, mixed Candida/bacterial bloodstream infections have shown significantly higher in-hospital mortality rates [18]. *Candida* spp. are known to form robust biofilms, which can enhance the survival and proliferation of bacterial pathogens such as *S. aureus* within the biofilm matrix, complicating treatment efforts [19,20].

The ability of bacteria to form biofilms on implant surfaces is a critical factor in the persistence of PJIs. Surface topography influences biofilm formation, with rough surfaces promoting higher biofilm development, which can shield bacteria from the immune response and antibiotics [21]. In addition, the high resistance rates of common PJI pathogens, such as *S. epidermidis*, to antibiotics such as methicillin and ciprofloxacin, pose significant treatment challenges. Resistance to fluoroquinolones, in particular, is associated with higher clinical failure rates [22]. Surgical debridement remains a cornerstone of PJI management, especially in early infections. However, the presence of multidrug-resistant organisms can lead to higher rates of clinical failure, underscoring the need for optimized surgical and antibiotic strategies [22]. Vancomycin and carbapenems are key components in this approach, providing effective coverage against Gram-positive and Gram-negative bacteria, respectively [23].

Current therapies to prevent and treat PJIs are far from ideal. In the case of irrigation of the prosthesis with antibiotics, the latter are washed away rapidly from the joint providing short antibacterial protection and can alter the biomechanical properties of the prosthesis [24]. In the case of the use of cement spacers, they can lead to joint dislocations and risk of fractures as they are intended for temporary use in the body but also, the antimicrobials loaded in the cement only elute in suitable concentrations for 24 h–48 h after insertion, followed by a very slow release pattern that can even trigger the appearance of resistance [25–30]. For example, AmB deoxycholate was incorporated in cements spacers resulting in a very low drug release (0.2 % after 24 h) [31]. Other approaches have explored the use of daptomycin and vancomycin-loaded poly-epsilon-caprolactone (PCL) microparticles [32] and PCL/Chitosan multilayer coatings to prevent PJIs [33] but with limited clinical translation.

Hence, there is an urgent clinical need to develop novel therapies that allow the prevention and treatment of bacterial and fungal PJIs. The hypothesis underpinning this work is that the administration of broad-spectrum antimicrobials encapsulated within bioadhesive microparticles could provide a longer sustained release to prevent and treat PJIs. Based on this premise, this work aimed to develop bioadhesive sustained-released microparticles combining vancomycin and amphotericin B (AmB) to prevent and treat both bacterial and fungal PJIs. Microparticles were adhered to the surface of the metallic hip prosthesis to assess drug release. Optimization studies along with an extensive particle characterization and evaluation of biological performance were carried out.

2. Materials and methods

2.1. Materials

Soluplus® and Kollicoat IR were donated from Basf (Ludwigshafen, Germany). Eudragit® RL 100 was provided by Evonik (Darmstadt, Germany) as a gift. Hyaluronic Acid was purchased from Merk (Mw: 170,000–250,000) (Madrid, Spain). Vancomycin (purity >90 %) was supplied by the Gregorio Marañón Hospital (Madrid, Spain) and AmB (purity >90 %) was purchased from Kemprotec Limited (Cumbria, UK). Commercial disks of vancomycin and AmB were purchased from Neo-Sensitabs (Rosco, Denmark). Salts and solvents (HPLC-grade) were purchased from Proquinorte (Madrid, Spain). Human albumin was obtained from Grifols® (Barcelona, Spain). All other chemicals and solvents were at least of ACS reagent grade and were used without further purification.

2.2. Preparation of microparticles: Design of experiment (DoE)

Two DoEs were carried out using the Software Design Expert® version 8.04 (Stat-Ease, Minneapolis, United States) to optimize the fabrication of microparticles containing AmB using spray drying. The combination of Soluplus®, Eudragit® RL100, and Kolicoat® IR was evaluated to target a sustained-drug release profile microparticles by spray drying.

2.2.1. Pre-screening DoE: Taguchi design

Seven variables with two levels with only eight experiments (L8 = 2^7) were established to determine which variables were most critical in the atomization process. Both the components of the formulation and the process parameters of the atomizer were taken into consideration including the amount of AmB (1 % or 5 %; *w/w*), the amount of Soluplus® (35 % or 65 % *w/w*), airflow (600 NL/h or 800 NL/h), inlet temperature (65 °C or 72 °C), vacuum aspiration (90 % or 100 %), liquid inlet velocity (5 mL/min or 15 mL/min) and time of sonication of the suspension before spray drying in a water bath at 10 W (5 min or 10 min).

In each experiment, the batch size was kept constant at 1g. Depending on the amount of AmB and Soluplus®, the remaining up to 1 g was completed with Eudragit® RL100. In 100 mL of ethanol, Eudragit® was first dissolved under continuous magnetic stirring. Afterward, AmB was dispersed in the mixture followed by the corresponding amount of Soluplus®. The mixture was kept under stirring for at least 15 min and then it was transferred to the water bath ultrasound for either 5 min or 10 min at 10 W. The obtained suspension with total solute content of 10 % (*w/v*) was spray-dried in a Buchi Spray drier B-190 (Labortechnik AG, Flawil, Switzerland) using the corresponding parameters from the DoE. After the process, the powder was immediately collected from the collector's vessel and stored in a desiccator under refrigerated conditions.

The responses evaluated were the yield of the process (%), the encapsulation of the AmB (%), the AmB aggregation state, and the antifungal activity. The matrix design of Taguchi DoE is shown in Table S1.

2.2.2. Surface response DoE: Box-Behnken design

Three variables were studied at three levels with a total of seventeen experiments (L17 = 3^3) to optimize the final formulation including the amount of AmB (5 %–7.5 % - 10 %; *w/w*), the amount of Soluplus® (50 %–65 % - 80 %%; *w/w*) and the liquid inlet velocity (10 mL/min - 15 mL/min - 20 mL/min). Based on the results obtained in the Taguchi design, several factors were kept constant in the Box-Behnken design

such as 700 NL/h airflow, 100 % aspiration, 10 min water bath sonication, and 70 °C inlet temperature. The matrix design of Box-Behnken DoE is shown in Table S2. As previously, the batch size was 1 g of total mass dispersed in 100 mL of ethanol. Eudragit® RL100 was added in sufficient quantity to complete 100 % of the formulation. Each sample was prepared as described in the previous section. The responses studied were yield (%), AmB encapsulation efficiency (%), and AmB aggregation state.

2.2.3. Formulation optimization and validation

The formulation was optimized aiming for the highest yield and AmB encapsulation efficiency. After optimization studies, the suggested formulation consisted of AmB as an API, Eudragit® RL100 as a controlled release excipient, and Soluplus® as a solubilizer.

After the optimization, preliminary drug release studies showed a too-prolonged release in aqueous media. Kollicoat® ^{IR} was incorporated into the mixture to counteract this effect. The resulting formulation included 27.5 % Eudragit® RL100, 50 % Soluplus®, 17.5 % Kollicoat® IR, and 5 % AmB (*w/w)*. Excipients and drug (1 g in total) were dispersed in methanol (100 mL) and the mixture was sonicated (10 min in a water bath) and then spray dried at 700 NL/h airflow, 100 % aspiration, 70 °C inlet temperature, and 12 mL/min liquid inlet velocity. Microparticles (50 mg) were mixed with hyaluronic acid (15 mg) and then dispersed in deionized water (0.7 mL) to form a gel-like structure to enhance the adhesive properties of the microparticulate formulation onto the metallic surface of the hip prosthesis. The same process parameters and formulation composition were utilized to encapsulate vancomycin within polymeric microparticles. A third combined formulation was prepared incorporating 5 % AmB and 5 % vancomycin (*w/w)*. The combined formulation was consisting of 5 % AmB, 5 % vancomycin, 50 % Soluplus®, 22.5 % Eudragit® RL100 and 17.5 % Kollicoat® IR (*w/w)*.

2.3. Characterization of the microparticulate formulation

2.3.1. Yield quantification

To determine the yield, the amount of product collected at the end of the atomization process compared to the initial mass was calculated with the following Equation (1):

$$Yield\ (\%) = \frac{Amount\ collected}{Total\ mass\ atomized} x\ 100 \qquad \text{(Equation 1)}$$

2.3.2. Quantification of AmB and vacomycin encapsulation by HPLC

The content of AmB and Vancomycin in the spray-dried microparticles were quantified using validated HPLC methods. Each spray-dried formulation (10 mg) was weighed and dissolved in 5 mL of methanol. The resulting solution was diluted 1:5 (*v/v*) with the respective mobile phase prior to HPLC analysis. AmB was quantified using a previously validated HPLC method by Espada et al., 2008 [34], using a Hypersil BDS column (200 mm × 4.6 mm, 5 μm), a mobile phase consisting of acetonitrile (AcN), acetic acid (AcOH) and water (52: 4.3: 43.7, *v:v:v*) at 1 mL/min flow rate, 50 μL injection volume and 406 nm wavelength [35]. AmB concentrations were determined by integrating the peak area at 6 min using a calibration curve. The linear calibration curve range was obtained over the range of 0.39 μg/mL to 100 μg/mL for unprocessed AmB, with an R^2 value of 0.9995 (y = 0.7627x – 0.1833).

For Vancomycin quantification, the previously validated HPLC method by de Jesús Valle et al., 2008 was used [36]. The mobile phase consisted of 50 mM ammonium phosphate: acetonitrile (92:8, *v: v*), with a final pH of 2.2, using a Nucleosil C18 column (250 mm × 4.6 mm, 5 μm) with a 0.7 mL/min flow rate and the injection volume of 40 μL. The detector was set at 205 nm [37,38]. A calibration curve between 50 μg/mL - 0.08 μg/mL for unprocessed Vancomycin was performed, with an R^2 value of 0.9998 (y = 1.6319x – 2.6633).

For drug encapsulation efficiency quantification (Equation (2)), approximately 5 mg of powder formulation (n = 3) was weighed and dispersed in 1 mL of the mobile phase and analyzed by HPLC using the respective method.

$$Encapsulation\ (\%) = \frac{Experimental\ amount\ of\ AmB}{Theoretical\ amount\ of\ AmB} x\ 100 \qquad \text{(Equation 2)}$$

2.3.3. Aggregation of AmB

Formulations were reconstituted and diluted as necessary with deionized water up to a theoretically 10 μg/mL AmB concentration. The resulting dilutions were scanned between 300 nm–450 nm (Shimadzu UV-1700 spectrophotometer) as previously described [35,39]. To calculate the AmB aggregation state, the ratio between the peak at 328 and 406 nm was taken into consideration according to Equation (3):

$$Aggregation\ ratio = \frac{Abs\ \lambda\ 328\ nm}{Abs\ \lambda\ 406\ nm} \qquad \text{(Equation 3)}$$

The wavelengths at 328 nm and 406 nm were chosen since they correlate with the AmB aggregation state, being the absorption at 328 nm characteristic of the dimeric state (oligomeric state) and the absorption at 406 nm of the monomeric state. If the aggregation ratio was greater than 1, this indicated a more aggregated AmB state while the opposite was indicative of a monomeric AmB predominance [40].

2.4. Physicochemical and solid-state characterization

2.4.1. Particle morphology

The morphology of the optimized microparticles containing AmB, vancomycin, or a mixture of both drugs was characterized by Scanning Electron Microscopy (SEM) using a JEOL6335F (Mussashime, Japan) with a voltage of 20 kV. A thin layer coating with gold was sputtered for 120 s on microparticles mounted on carbon-coated tubs using a QUORUM Q150R S (Mussashime, Japan) to help conductivity. Also, SEM analysis was carried out on the combined AmB/vancomycin microparticles reconstituted with hyaluronic acid and deionized water. The gel was spread over a stub and left overnight to dry at room temperature before analysis.

2.4.2. Powder X-ray diffraction (pRXD)

Powder X-ray analysis was carried out using a Philips®X'Pert-MPD X-ray diffractometer (Malvern Panalytical®; Almelo, The Netherlands) equipped with Ni-filtered Cu K radiation (1.54). A 40 kV voltage and 40 mA current were used to perform the study. PXRD patterns were recorded at a step scan rate of 0.05° per second from 5° to 40° on the 2-theta scale (n = 3) [41]. Physical mixtures of raw powder materials between API and excipients were carried out in an agate mortar and pestle for comparison purposes.

2.4.3. Differential scanning calorimetry (DSC) and thermogravimetric analysis (TGA)

DSC and TGA analysis were performed simultaneously on an SDT Q600 instrument (TA Instruments, Elstree, UK) with nitrogen as the purge gas. The samples (4–6 mg) were weighted and heated at a rate of 10 °C/min, ranging from 25 °C to 500 °C. The instrument was calibrated with indium as the reference standard (n = 3). TA Universal analysis software v 4.5A (Waters, USA) was used for data collection and analysis.

2.4.4. Fourier-transform infrared (FT-IR) spectroscopy

FT-IR analyses were conducted using a Nicolet Nexus 670–870 (Thermofisher®, Madrid, Spain). Infrared spectra were recorded in the range of 400 cm^{-1} – 4000 cm^{-1} with a 1 nm step scan. The data were interpreted using Spectragryph (version 1.2.9, Oberstdorf, Germany) software, and data normalization was carried out.

2.5. Haemolysis studies

Venous blood was obtained from a healthy 27-year-old male volun-

teer (5.48×10^6 RBC/mL) and collected into a K2-EDTA-coated Vacutainer tube to prevent coagulation. Haemolysis studies were performed as previously described [42,43]. Briefly, blood was centrifuged (5 min at 1000 g) and the haematocrit and plasma levels were marked on the tube. The supernatant was discarded, and the tube was refilled with 150 mM NaCl solution. The RBCs were washed twice. After the last wash, the supernatant was discarded, and the RBCs were diluted to 4 % concentration using PBS at pH 7.4. The diluted RBCs were added to a 96-well plate (180 μL/well). Stock solutions of the three microparticulate formulations (AmB, vancomycin, and AmB-vancomycin-loaded formulations) were prepared with a drug concentration ranging from 50 mg/mL – 0.5 mg/mL using deionized water. As a comparison, a standard solution of each drug in DMSO at the same concentrations was tested. Samples (20 μL) from each concentration were loaded into the wells in triplicate. For positive control wells, a 20 % solution of Triton X-100 (20 μL) was utilized. For negative control wells, PBS at pH 7.4 (20 μL) was incorporated. Plates were incubated at 37 °C for 1 h. Afterward, plates were centrifuged at 2500 rpm for 5 min to pellet intact RBCs, and 50 μL of the supernatant from each well was transferred into a clear, flat-bottomed 96-well plate. The absorbance of the supernatants was measured using a plate reader (BioTek, ELx808) at 570 nm. The percentage of haemolysis was calculated using Equation (4):

$$\text{Haemolysis}\ (\%) = \frac{(\text{ABS}_{\text{sample}} - \text{ABS}_{\text{PBS}})}{(\text{ABS}_{\text{Triton}} - \text{ABS}_{\text{PBS}})} \qquad \text{(Equation 4)}$$

Where ABS sample is the absorbance value of each sample, ABS PBS is the absorbance value of PBS and ABS Triton is the absorbance value of Triton [42].

2.6. Preparation and characterization of the hydrogel

2.6.1. Adhesion studies

Fifty milligrams of the microparticles were mixed with 15 mg of hyaluronic acid followed by the addition of 0.7 mL of deionized water. The mixture was stirred until a homogenous bioadhesive gel was formed. The gel (1 g quantity) was spread over the surface of a femoral stem (10 cm^2) and the time needed for full dryness was quantified.

Drying time assessment was performed by applying the hydrogel uniformly across the prosthesis surface and monitoring until complete desiccation, which occurred within 5–7 min at room temperature. The gel formulation, designed for optimal extensibility across prosthetic surfaces, demonstrated consistent adhesion without observable changes in elution profiles or surface sloughing. While excipient composition in the microparticles may influence drying kinetics, no significant variations were observed under standardized application conditions.

2.6.2. Rheological characterization

Flow viscosity of the bioadhesive gels was evaluated in triplicate using a Rheometer Brookfield (Middleborough, MA, USA) Model DV-III fitted with a temperature control probe. A 5-cm cone–plate measuring geometry was used (Spindle CP-42). The temperature of all the measurements was maintained at 25 °C. Viscosity (cP) and shear stress (D × cm^{-2}) were determined over a speed rate ramping from 0 rpm to 0.5 rpm and from 0.5 rpm to 0 rpm, and a shear rate from 0 (1/s) to 1.92 (1/s). Before measurements, a standard was analyzed. The fluidity parameter was calculated using linear regression from the slope of the shear stress versus shear rate plot.

2.7. Drug release

The microparticles (50 mg) containing AmB, vancomycin, or both drugs were mixed in a mortar and pestle with 15 mg of hyaluronic acid and were dispersed in 700 μL of deionized water. The mixture was manually mixed until a homogenous gel was obtained which immediately was spread over a 10 cm^2 over the surface of a femoral stem. The femoral stem prosthesis with the bioadhesive gel adhered and dried on the surface was immersed in a 3D printed container using cyclic olefin copolymer to minimize particle adsorption and with similar dimensions to the prosthesis to mimic the bone microenvironment, with a capacity for 20 mL of liquid that consisted of a mixture of PBS buffer pH 7.4 with human albumin (80:20, *v: v*). The addition of albumin to the medium was crucial, considering the high plasma protein binding of AmB and vancomycin. The experiment was performed in triplicate. The container was covered with parafilm to prevent evaporation of the medium and was kept at 37 °C for 120 h. Samples (750 μL) were withdrawn at different times (0, 0.5 h, 1 h, 3 h, 5 h, 7 h, 9 h, 12 h, 24 h, 48 h, 36 h, 72 h and 120 h) and then were further diluted with methanol (1:1, *v:v*). The volume was replaced with a fresh 750 μL medium to maintain sink conditions. Collected samples were frozen for 24 h at −20 °C to precipitate proteins before HPLC analysis. Subsequently, samples were centrifuged at 10,000 rpm for 15 min and the supernatant (300 μL) was analyzed by HPLC.

Table 1
Storage conditions of the long-term and accelerated stability studies (RH, relative humidity).

Group	Storage conditions	Time points
Accelerated	40 ± 2 °C/75 % RH ± 5 % RH 50 ± 2 °C/75 % RH ± 5 % RH 50 ± 2 °C/10 % RH ± 5 % RH 60 ± 2 °C/10 % RH ± 5 % RH 70 ± 2 °C/10 % RH ± 5 % RH 60 ± 2 °C/50 % RH ± 5 % RH	3, 8, 16, 22 days
Long-term	25 ± 2 °C/60 % RH ± 5 % RH 4 ± 3 °C/10 % RH ± 5 % RH	3, 6, 9, 12 months

2.8. Long-term and accelerated stability studies

The optimized microparticles containing either AmB or vancomycin (10 mg) were placed in uncapped HPLC vials and introduced into test Cuspor stability chambers exposed to different conditions of temperature and humidity (Table 1). The desired humidity was achieved by using Cuspor humidity capsules (Cuspor Ltd., Ireland) which were placed into the chamber, which in turn were put inside ovens at the selected temperature to ensure that the RH equilibrium was reached before the aging of the formulations [44,45]. A sensor cap was introduced to the test chamber to collect the temperature and humidity test conditions wirelessly. At different time points, samples were collected and analyzed by HPLC for chemical degradation. A humidity-corrected Arrhenius equation was used to estimate the effect of temperature and RH on degradation rates (Equation (5)) [46]:

$$LnK = LnA - \frac{Ea}{RT} B(RH) \qquad \text{(Equation 5)}$$

Where K is the degradation constant, A is the collision frequency, Ea is the activation energy, B(RH) is the humidity sensitivity factor, T is the absolute temperature and R is the gas constant. Different fitting methods/models were assessed: Avrami, diffusion, first order, second order, and zero order. The model with the highest R^2 was selected for shelf-life prediction at a mean kinetic temperature of 25 °C and 60 % relative humidity and under refrigerated conditions [47].

2.9. Antibacterial in vitro assay

The antibacterial effect of the loaded microparticles was tested against *Staphylococcus epidermidis* (ATCC 12228) and *Staphylococcus aureus* (ATCC 23235). The antimicrobial activity was tested by diffusion assay in Kirby-Bauer agar [43]. Microparticles with vancomycin and the combination of both APIs dispersed in deionized water were loaded onto 6 mm in diameter paper discs and placed in the center of agar plates.

Commercial discs of vancomycin (30 μg, Neo-Sensitabs, Rosco, Denmark) were used as a positive control. A vancomycin raw material in the same concentrations as in the formulation (10 μg) was used also as a control. Inhibition zone diameters were measured at points where there was complete inhibition of bacterial growth after 24 h of incubation. Isolates were classified as vancomycin susceptible (S) when the zone of inhibition was greater than 15 mm according to the CLSI guidelines.

Minimum Inhibitory Concentration (MIC) was evaluated as previously described (28). Cultures were prepared by picking a single colony from a 24-h Mueller-Hinton agar (MHA) plate and re-suspending it in 5 mL of Mueller Hinton Broth (MHB). Afterward, cultures were grown aerobically for 20 h at 37 °C with shaking at 200 rpm. The cultures were diluted with fresh MHB with a 0.1 absorbance at 600 nm, corresponding to 10^6 colony forming units (CFU)/mL based on 0.5 McFarland standard. The suspension was further diluted with MHB up to a concentration of 4 × 10^5 CFU/mL.

Microparticles with vancomycin and a combination of both drugs were dispersed in 6 different volumes of MHB to obtain concentrations ranging from 2 μg/mL to 64 μg/mL respectively. The inoculum (50 μL) containing 2 × 10^4 CFU was added to the solution, except in medium growth for the control tubes. As a positive control for bacterial growth, the bacteria were grown in MHB. Tubes were incubated at 37 °C with shaking at 180 rpm for 24 h. The turbidity of the tubes was visually checked. Additionally, to calculate the MIC, 10 μL from each tube was cultured on MHA plates and was further incubated for 24 h at 37 °C (drop plate method). The MIC was determined as the lowest concentration with an absence of colony growth [48].

2.10. Antifungal in vitro assay

The antifungal activity was evaluated by agar diffusion assay with different species of *Candida* sp. (*C. albicans* CECT 1394, *C. parapsilosis* 57744, *C. glabrata* 60750, and *C. krusei* 1068) [39,49]. Microparticles with AmB and the combination of both drugs (AmB and vancomycin) were dispersed in deionized water and loaded onto 6 mm in diameter paper discs and placed in the center of the agar plate. Discs loaded with AmB dissolved in DMSO (10 μg) and commercial discs of AmB (10 μg, Neo-Sensitabs, Rosco, Denmark) were used as a positive control. After 48 h, inhibition zone diameters were measured at points where complete inhibition of fungal growth was observed. Isolates were classified according to the Clinical & Laboratory Standards Institute (CLSI) as AmB susceptible (S) when the zone of inhibition was greater than 15 mm; resistant (R), if the zone of inhibition was lower than 10 mm; and intermediate (or dose-dependent) (I) if the zone of inhibition was between 11 and 14 mm.

The MIC was also evaluated. Cultures were prepared by picking a single colony from a 24-h MHB plate and resuspending with 0.9 % sterile physiological saline solution to achieve 0.1 absorbance at 600 nm, corresponding to 10^6 CFU/mL based on the 0.5 McFarland standard. The suspension was further diluted with MHB up to a concentration of 4 × 10^5 CFU/mL.

Microparticles with AmB and a combination of both drugs were dispersed in MHB in 6 different concentrations from 2 μg/mL to 64 μg/mL. The inoculum (50 μL) containing 2 × 10^4 CFU was added to the solution (2 mL), except in the medium growth that was used as a control tube. As a positive control for bacterial growth, a tube just containing MHB, and bacteria inoculum was prepared. Tubes were incubated at 37 °C with shaking at 180 rpm for 24 h. The turbidity of the tubes was visually checked. Additionally, to calculate the MIC, 10 μL from each tube was cultured on MHA plates and was further incubated for 24 h at 37 °C (drop plate method) [48]. The MIC was determined as the lowest concentration with an absence of colony growth.

2.11. Cytotoxicity studies

2.11.1. Cell culture

The human osteosarcoma cell line Saos-2 (HTB - 85™), the human fibroblast cell line BJ (CR-2522™), and the human fetal osteoblastic cell line hFOB 1.19 (CRL - 11372™) were obtained from the American Type Culture Collection (ATCC®). The Saos-2 cells were cultured in Dulbecco's Modified Eagle Medium (DMEM) (Lonza, Basel, Switzerland) containing 10 % fetal bovine serum (FBS) (Linus) and 1 % penicillin/streptomycin (HyClone Cytiva, Austria). The BJ cells were grown in Eagle's Minimum Essential Medium (HyClone Cytiva, Austria) supplemented with 10 % FBS and 1 % penicillin/streptomycin. The hFOB cells were cultured in a 1:1 mixture of Ham's F12 and DMEM without phenol red (HyClone Cytiva, Austria) containing 10 % FBS and 1 % geneticin. These cell lines were maintained in a humidified atmosphere of 95 % air and 5 % CO_2 at 37 °C. Saos-2, BJ, and hFOB 1.19 cells were treated with microparticles loaded with vancomycin, AmB, and vancomycin/AmB at a concentration of 60 μg/mL for 24 h, 72 h, and 1 week. The selection of this concentration was based on the maximum drug concentration achieved during the release studies.

2.11.2. Cell viability assay

The effect of microparticles loaded with vancomycin, AmB and vancomycin/AmB, and the corresponding drugs on cell viability was determined using the 3-(4,5-dimethyl-thiazol-2-yl)-2,5-diphenyl-tetrazolium bromide (MTT) method (Mosmann, T., 1983). Briefly, Saos-2 and BJ cells were seeded onto 24-well plates at a density of 10^5 cells per well and hFOB 1.19 cells at a density of 10^6 cells per well. Microparticulate formulations (1 mg) were mixed with 0.3 mg of hyaluronic acid and 40 μl of deionized water. Formulations were further diluted with 200 μl of media and then were added on top of 0.4 μm inserts. Cell viability was evaluated at 24, 72 h and 1 week.

At the later time points, an MTT stock solution (2 mg/mL in PBS) was added and incubated for 1 h. After incubation, the produced formazan crystals were dissolved using 100 μL per well DMSO. The absorbance was finally determined at 550 nm by using a Spectrostar BMG microplate reader (BMG Labtech Inc., Ortenberg, Germany). Cell viability was expressed as a percentage compared to control cells.

2.12. Evaluation of cell morphology by Scanning Electron Microscopy (SEM)

Saos-2, BJ, and hFOB 1.19 cells were seeded onto collagen-coated (1:10 dilution, *v:v*) dishes. Cells were then treated with microparticles loaded with AmB, vancomycin, and AmB/vancomycin as well as with AmB or vancomycin for 1 week. After the incubation period, cells were washed two times with phosphate-buffered saline (PBS) and with ultrapure water. Then, cells were dehydrated for 10 min with increasing concentrations of ethanol (50 %, 70 %, 80 %, 90 % and 99.9 % concentrations). Critical drying point was then performed using a LeicaEM CPD300 Critical Point Dryer (Leica Mikrosysteme Vertrieb GmbH, Wetzlar, Germany). Samples were sputter-coated with gold and were examined with a scanning electron microscope (JEOL JSM 6400, Tokyo, Japan) with a 20 kV acceleration voltage.

2.13. Statistical analysis

Minitab 19 (Minitab Ltd., Coventry, UK) was used for statistical analysis. The one-way ANOVA test was performed for the release, haemolysis, antifungal and antibacterial, and cytotoxicity *in vitro* assays. *p*-values below 0.05 were considered statistically significant differences. The results were plotted using Origin 2021 (OriginLab Corporation, Northampton, MA, USA).

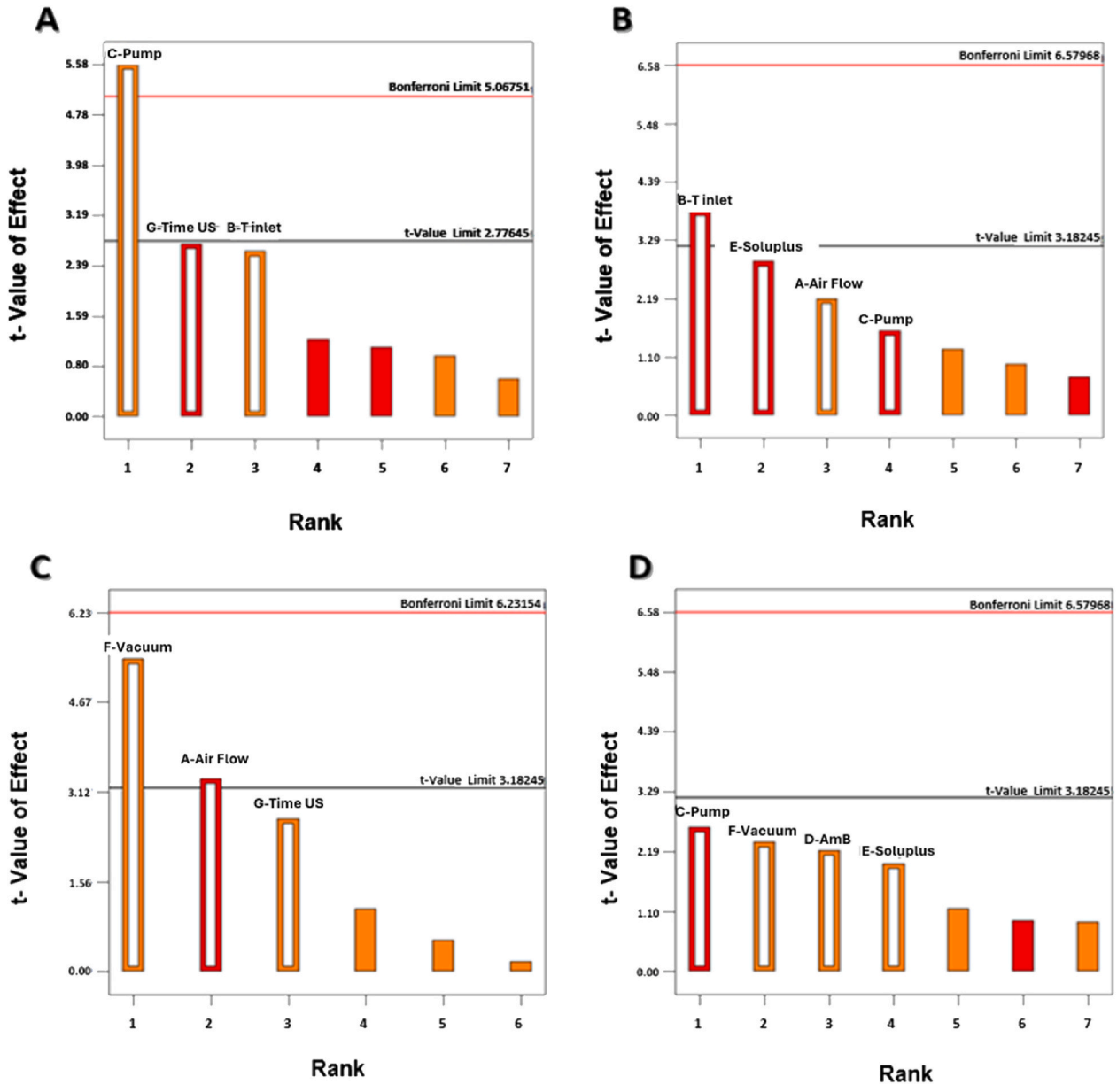

Fig. 1. Pareto charts depicting the influence of the seven factors (7 bars) assessed on the Taguchi DOE design. Key: **(A)** Yield (%); **(B)** AmB encapsulation efficiency **(C)** AmB aggregation state; **(D)** AmB efficacy expressed as inhibition halo against *C. albicans*. Orange bars represent a positive effect of the factor on the response while red bars represent a negative effect. (For interpretation of the references to colour in this figure legend, the reader is referred to the Web version of this article.)

3. Results

3.1. Preparation of microparticles: Design of experiment (DoE)

The screening of various formulation and process parameters was performed using a Taguchi design for seven factors at two levels each. Implementation of the design is useful for identifying the most significant factors with minimum experimentation and saving time, effort, and materials. This design has the specific advantage of requiring minimal runs for many independent variables (Table S1). Preliminary screening embarks upon the phenomenon of the "sparsity effect", in which only a few of the factors among numerous envisioned ones truly explain a large proportion of the experimental variation [45]. In Fig. 1, Pareto charts illustrate the most influential variables during the spray drying process being depicted as orange bars those factors that affect positively the Critical Quality Attributes (CQAs) of the microparticles, and in red those that affect negatively.

The yield was favored when a higher liquid velocity (pump) was used while the AmB encapsulation efficiency was reduced at higher inlet temperature. Temperature is a critical factor since Soluplus® can increase its stickiness if the working temperature goes above its glass transition temperature. However, the temperature should be kept above the evaporation temperature of the solvent used to ensure suitable drying conditions. Based on this, the inlet temperature was kept at 70 °C for the Box-Behnken second DoE design. The aggregation state was impacted positively when a high vacuum was used being opposite for the airflow. At higher airflows, the solvent evaporates faster, and particles tend to aggregate less. Regarding, the efficacy against *C. Albicans*, no significant factors were found in the Taguchi design as all formulations exhibited halos above 15 mm in diameter.

3.1.1. QbD-based model development and response surface analysis

Polynomial analysis was carried out by a multilinear regression analysis method suggesting that the linear model was the best fit for the

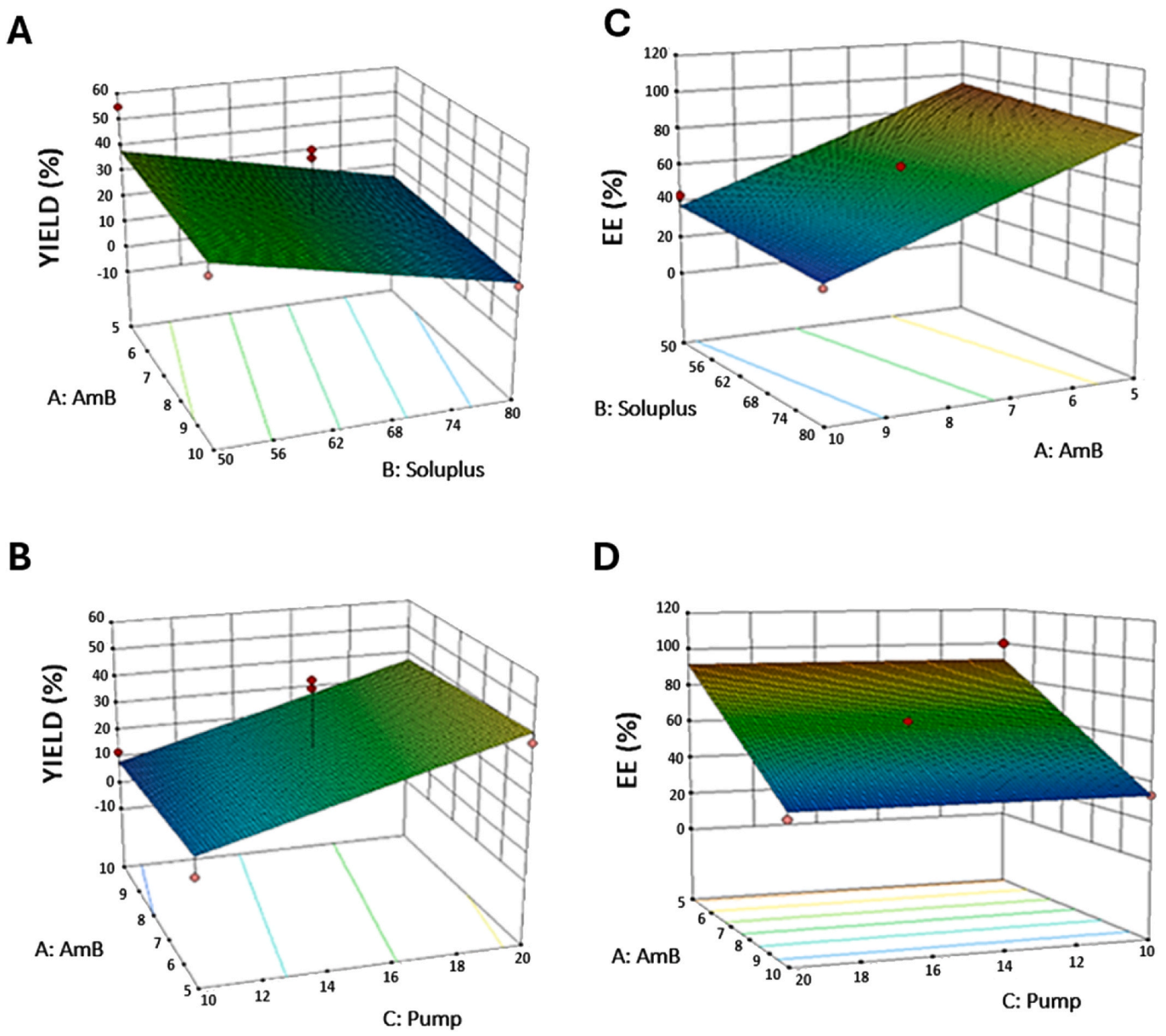

Fig. 2. 3D response surface showing the influence of the amount of AmB, the amount of Soluplus, and the liquid velocity on the yield **(a,b)** and AmB encapsulation efficiency **(c,d)**.

yield and drug encapsulation responses. The coefficients of the model equations generated for each CQA revealed the goodness of fit of the experimental data to the selected model with high values of R^2 and low p-values <0.05 for the latter responses while no significant differences were observed for the AmB aggregation state.

The yield of the process increased significantly when lower amounts of Soluplus® were used which can be related to the low T_g of the excipient impacting its processability during spray drying. However, higher liquid velocity rates increased the yield while AmB content had no significant impact. The encapsulation efficiency was drastically reduced when greater amounts of AmB were used. The amount of Soluplus® and the liquid velocity did not impact significantly on drug encapsulation (Fig. 2).

3.1.2. Search for the optimum formulation and validation of QbD

The search for an optimum formulation was performed by trading-off various CQAs to attain the desired objectives giving priority to the maximization of AmB encapsulation efficiency and yield. Based on the aforesaid objectives, the optimized formulation was 5 % of AmB and 50 % of Soluplus®. The remaining formulation consisted of 45 % of Eudragit RL100. The following optimized processing factors were: 20 % liquid velocity equivalent to 12 mL/min, 70 °C T inlet, 100 % vacuum, and 700 NL/h airflow. Validation of the QbD methodology revealed proximity between the predicted values of the responses (90 % confidence intervals) with observed ones for prepared check-point formulations: 52.86 % yield (51.80 %–54.89 %), 95.6 % drug encapsulation (74 %–100 %) and 0.79 aggregation rate (0.78–0.81).

After carrying out a preliminary set of drug release studies, the release was too prolonged (>7 days), and hence, the optimized formulation was modified by reducing the EudragitRL100 amount to 27.5 % and including 17.5 % of Kollicoat IR to accelerate the drug release profile. The same microparticle formulation was prepared replacing the amount of AmB with vancomycin. A combined formulation with 5 % AmB and 5 % vancomycin along with 50 % Soluplus, 22.5 % Eudragit RL100, and 17.5 % Kollicoat IR was also prepared. The yield, drug encapsulation, and aggregation states were within the confidence

Table 2
Summary of the physicochemical properties of optimized microparticles.

Formulation	Yield (%)	Drug Loading (%)	Encapsulation Efficiency (%)
AmB-loaded microparticles	52.9 ± 1.6	4.8 ± 0.8	95.6 ± 15.9
Vancomycin-loaded microparticles	54.6 ± 9.3	4.5 ± 1.1	93.0 ± 12.8
AmB/Vancomycin-loaded microparticles	53.0 ± 14.1	4.7 ± 1.4 (AmB) 4.6 ± 1.7 (Vanco)	94.3 ± 10.6 (AmB) 92.8 ± 7.9 (Vanco)

intervals from the DoE model generated (Table 2).

3.2. Characterization of the microparticulate formulation

3.2.1. Morphology

SEM micrographs showed microparticles with a particle size ranging from 1 μm–10 μm (Fig. 3). No crystals were observed on the surface of the particles. However, the surface of the particles was collapsed with multiple angular faces which may enhance its surface area and points of contact upon reconstitution and spread over the surface of the femoral stem. Fig. 3d illustrates how the particles upon reconstitution with hyaluronic acid and deionized water maintain intact spherical shape.

3.2.2. Solid state characterization

pXRD pattern of the loaded microparticles as well as excipients, unprocessed materials, and physical mixtures are illustrated in Fig. 4A. Significant differences were observed between the two APIs, being AmB a crystalline raw powder material while vancomycin was fully amorphous. A characteristic amorphous halo was observed for both microparticulate formulations in contrast to the physical mixture containing AmB in which characteristic Bragg peaks attributed to AmB were observed.

The FTIR spectra show broad bands for all the components especially those in the amorphous state (Fig. 4B). Characteristic bands were observed at 1732 cm^{-1} and 1629 cm^{-1} in both the AmB and vancomycin microparticulate formulations which are attributed to the C=O stretching for the ester and the tertiary amide of the Soluplus® excipient. Due to the low amount of AmB and vancomycin in the microparticles, specific bands were not observed in the final formulation. However, differences were found between physical mixtures and microparticulate formulations, the latter with broader peaks attributed

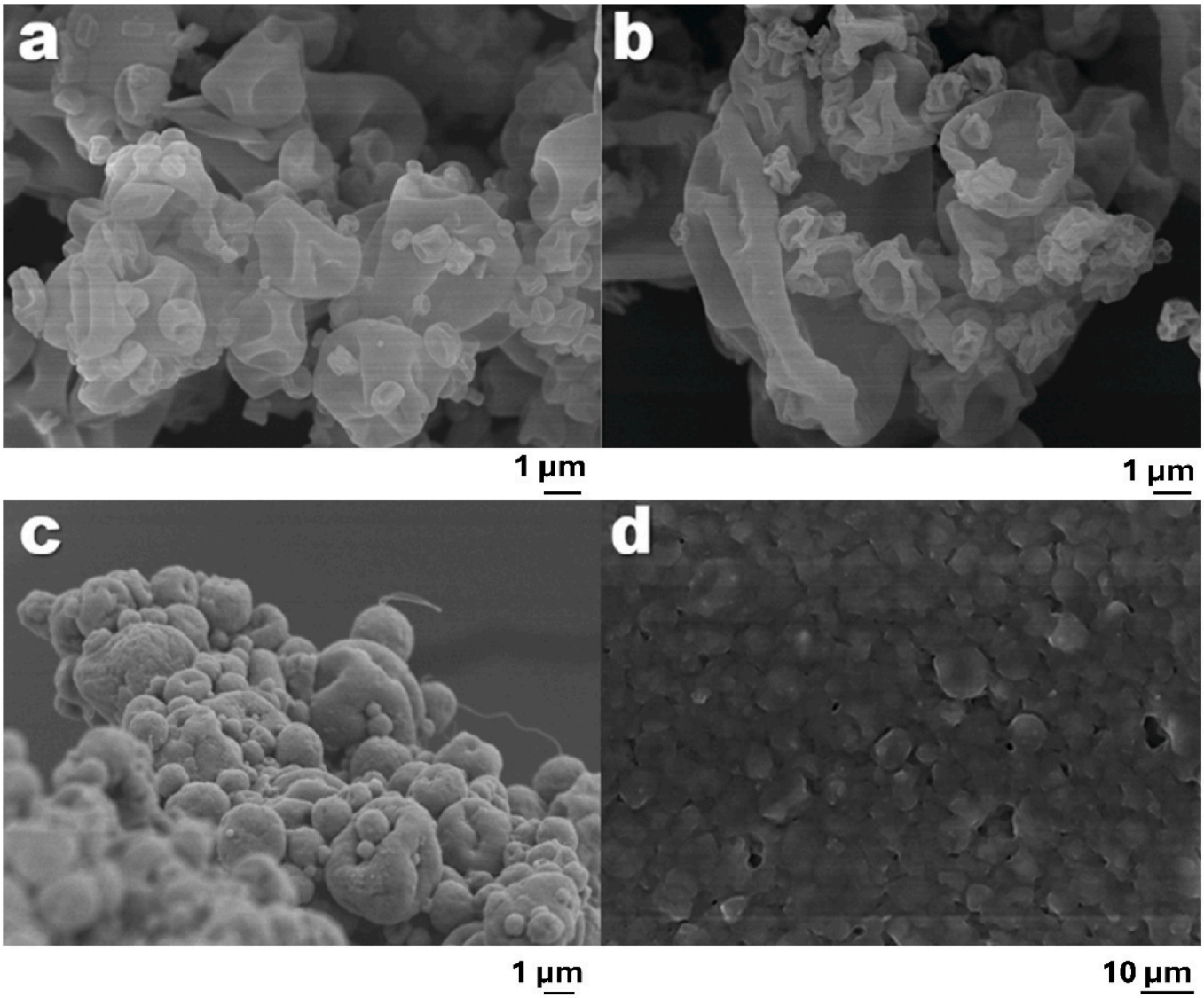

Fig. 3. SEM micrographs of spray-dried microparticles. Key: **(a)** AmB microparticles, **(b)** Vancomycin microparticles; **(c)** AmB/vancomycin loaded microparticles; **(d)** AmB/vancomycin microparticles after reconstitution with hyaluronic acid and spread over the prosthesis surface.

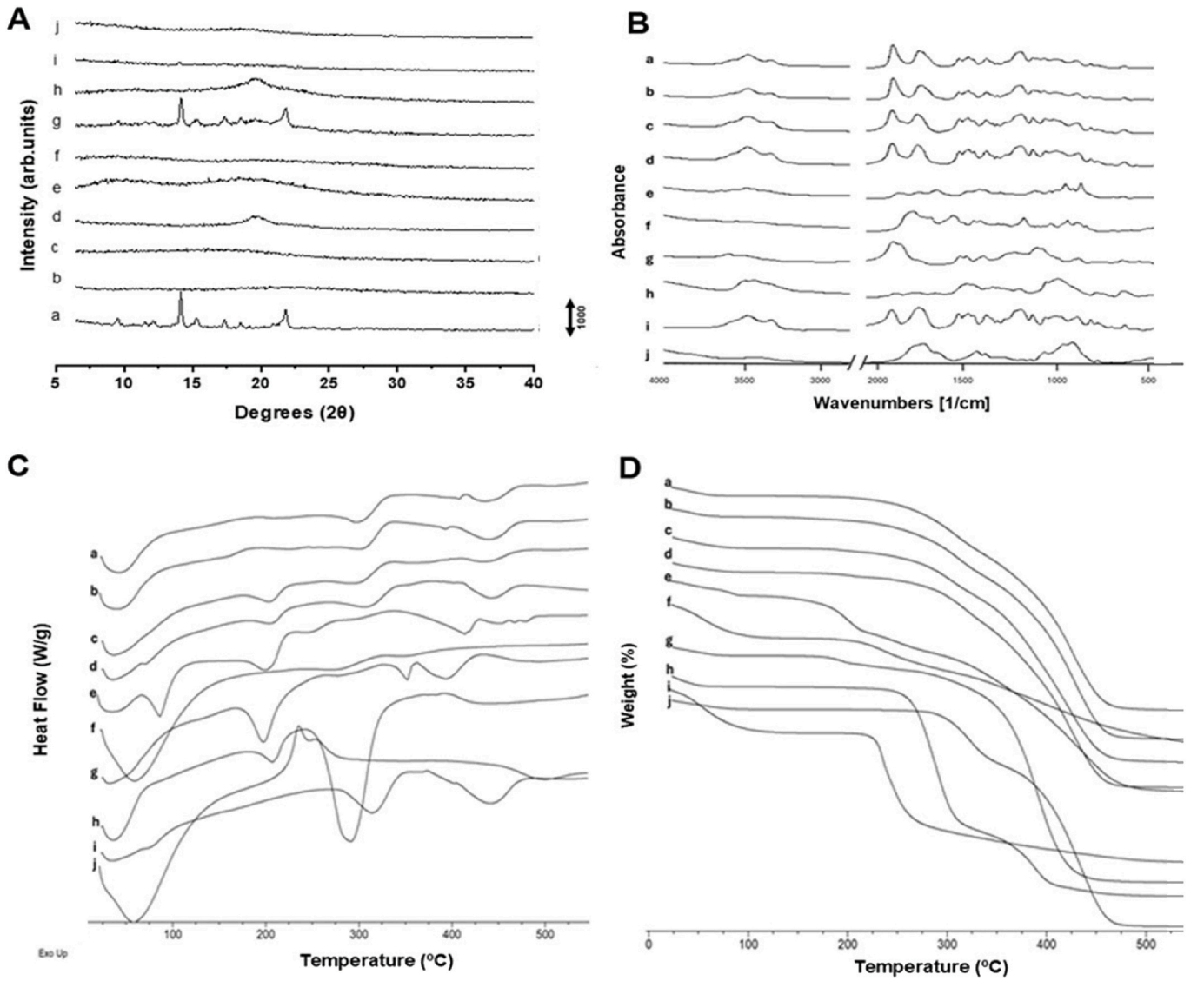

Fig. 4. Physicochemical characterization of microparticulate formulations and unprocessed materials. A. pXRD analysis of microparticulate formulations. **Key**: **a)** AmB raw material; **b)** Vancomycin raw material; **c)** Eudragit® RL100; **d)** Kollicoat® IR; **e)** Soluplus®; **f)** Hyaluronic acid; **g)** Physical mixture between the excipients and AmB; **h)** Physical mixture between the excipients and vancomycin; **i)** AmB microparticles and **j)** Vancomycin microparticles. **B. FTIR analysis**, **C. DSC analysis** and, **D. TGA analysis**. **Key**: **a)** Vancomycin loaded microparticles; b) AmB loaded microparticles; **c)** Physical mixture between the excipients and vancomycin; **d)** Physical mixture between the excipients and AmB; **e)** AmB raw material; **f)** Vancomycin raw material; **g)** Eudragit® RL100; **h)** Kollicoat® IR; **i)** Hyaluronic acid and **j)** Soluplus®.

to its amorphous nature. It is worth highlighting the strong bands at 2853 cm^{-1} and 2929 cm^{-1}, attributed to O-H stretching and the formation of H-bonds between drugs and excipients.

The thermal analysis for all the formulations and unprocessed materials is shown in Fig. 4C–D. In the case of AmB, two endothermic peaks were recorded at around 100 °C and 200 °C (Fig. 4C). Similar peaks were found in the physical mixture between AmB and unprocessed excipients. However, the endothermic events attributed to AmB were not present in the AmB-loaded microparticulate formulations which aligns with the pXRD results evidencing its amorphous nature (Fig. 4A). In the case of vancomycin, the unprocessed material was amorphous and did not show any endothermic event. However, the physical mixture between vancomycin and excipients showed two endothermic events which may be related to the degradation of Eudragit RL100 (~200 °C) and the Soluplus®-hyaluronic acid (~250 °C – 280 °C). Only the second thermal events were found in the vancomycin-loaded microparticles which correlates with better thermal stability as indicated in the TGA analysis (Fig. 4D). Similar thermal stability was found for the AmB-loaded microparticles, which was better than the individual components.

3.3. Haemolysis assay

The HC_{50} (haemolytic concentration that produces 50 % haemolysis of exposed red blood cells) for AmB, vancomycin, and AmB/vancomycin microparticles were 99.16 μg/mL, 61.25 μg/mL and, 99.16 μg/mL respectively while the HC_{50} for AmB dissolved in DMSO was 22.55 μg/mL and, for the vancomycin, the toxicity values were above of the highest concentration (50 μg/mL) tested. The encapsulation of AmB in the microparticles showed a significant reduction in the haemolytic toxicity of the drug ($p < 0.05$). HC_{50} was 4.3 times lower after the AmB encapsulation within microparticles. This is a key factor in developing parenteral formulations of AmB, as the main adverse effect limiting therapy along with its nephrotoxicity [35,50]. The encapsulated AmB showed a sustained drug release profile in an aqueous medium which means that the toxicity is limited upon administration in contact with physiological fluids. The same protective effect was observed for the

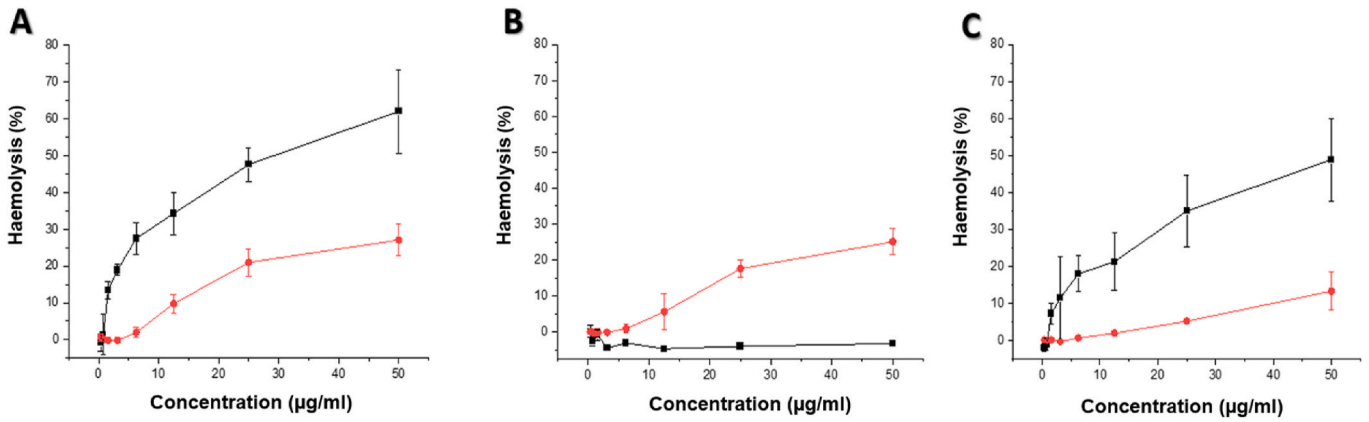

Fig. 5. Haemolytic toxicity of microparticulate formulations compared with the active ingredients dissolved in DMSO. Key: **A)** (—■—)AmB (—●—)AmB microparticles; **B)** (—■—)Vancomycin (—●—)Vancomycin microparticles and, **C)** (—■—) AmB and vancomycin (—●—) Combined microparticles with vancomycin and AmB.

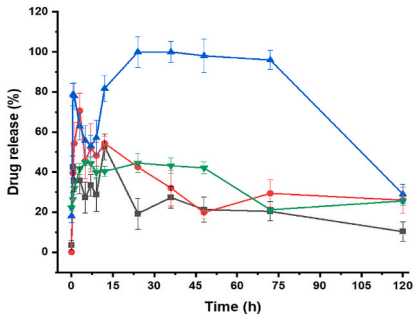

Fig. 6. Drug release after application of the bioadhesive gel on the surface of the femoral stem. Key (—■—): Amount of AmB released from microparticles loaded with AmB (—●—), Amount of AmB released from microparticles loaded with vancomycin and AmB (—▲—); Amount of vancomycin released from vancomycin microparticles, and (—▼—) Amount of vancomycin released from vancomycin and AmB microparticles.

combined AmB/vancomycin microparticulate formulation. A 5-fold reduction in the HC_{50} was observed. However, this protective effect was not found with vancomycin microparticles considering that this drug is not haemolytic. Vancomycin microparticles were more haematotoxin, due to the combined effect of the excipients that are acting as surfactants on the RBCs (Fig. 5).

3.4. Preparation and characterization of the hydrogel

After reconstitution of the microparticles in deionized water and hyaluronic acid, a bioadhesive gel was formed which was easily spread on the surface of the femoral stem. The drying time was below 10 min ($n = 3$) which facilitates its administration during the surgical procedure.

3.5. Drug release

The three microparticulate formulations showed a sustained release profile marked by a burst release ranging from 40 % to 80 % depending on the drug over the first 10 h followed by a prolonged sustained release over 7 days (Fig. 6). After 24 h, drug concentration in the medium was reduced which can be due to a parachute effect, especially for AmB whose aqueous solubility is very low. Albumin was added to the medium to compensate for the poor AmB aqueous solubility. In the case of vancomycin, drug stability in aqueous media was poor showing fast degradation (1 % of drug degraded per day, data not shown). The release profile of a single drug-loaded microparticle was significantly different from those combined ones (p-value <0.05). AmB-loaded microparticles had a more prolonged release in comparison to the combined-loaded microparticles while the opposite effect was observed for the vancomycin (faster release with the vancomycin-loaded microparticles compared to the dual formulation). This indicates an interaction between both drugs when they are co-formulated together.

Table 3
The correlation coefficient, activation energy, and degradation kinetics of amB and vancomycin microparticulate formulations.

Formulation	Condition	Correlation coefficient *(R)*	*Ea* (kcal/mol)	Degradation kinetic model
Vancomycin-loaded microparticles	With RH	0.903	14.51	Avrami
	Without RH	0.978	9.59	
AmB-loaded microparticles	With RH	0.887	14.82	Zero
	Without RH	0.994	7.42	

3.6. Accelerated and long-term drug stability

The kinetic model that showed the best fit for the experimental data points at different conditions for AmB-loaded microparticles was zero-order, while Avrami fitted the degradation profile for vancomycin-loaded microparticles ($R > 0.9$). The degradation rate using either the Avrami or zero-order reaction for both microparticles at different temperatures was employed to extrapolate the activation energy (Ea) from the Arrhenius equation. The activation energy for both formulations was significantly higher in the presence of RH than without RH, indicating better chemical stability (Table 3). This can be attributed to a solid-state transition upon exposure to RH, such as a physical transformation from amorphous to crystalline state, which indicates the need for desiccated conditions during storage for both formulations. From the Arrhenius equations, the iso-conversion time considering a specification limit of 10 % degradation at 4 °C under desiccated conditions for AmB and vancomycin microparticles was 401 days and 214 days, respectively.

Long-term stability studies showed that vancomycin-loaded microparticles were chemically stable for at least 100 days at 4 °C/10 % RH and at least 250 days at 25 °C/60 % RH (drug content >90 %). This indicates the susceptibility for crystallization for vancomycin-loaded microparticles which explains the solid-state transformation from amorphous to crystalline and hence, the increase in chemical stability at 25 °C compared to refrigerated conditions. AmB microparticles remained stable for more than one year at 4 °C/10 % RH and 25 °C/60 %

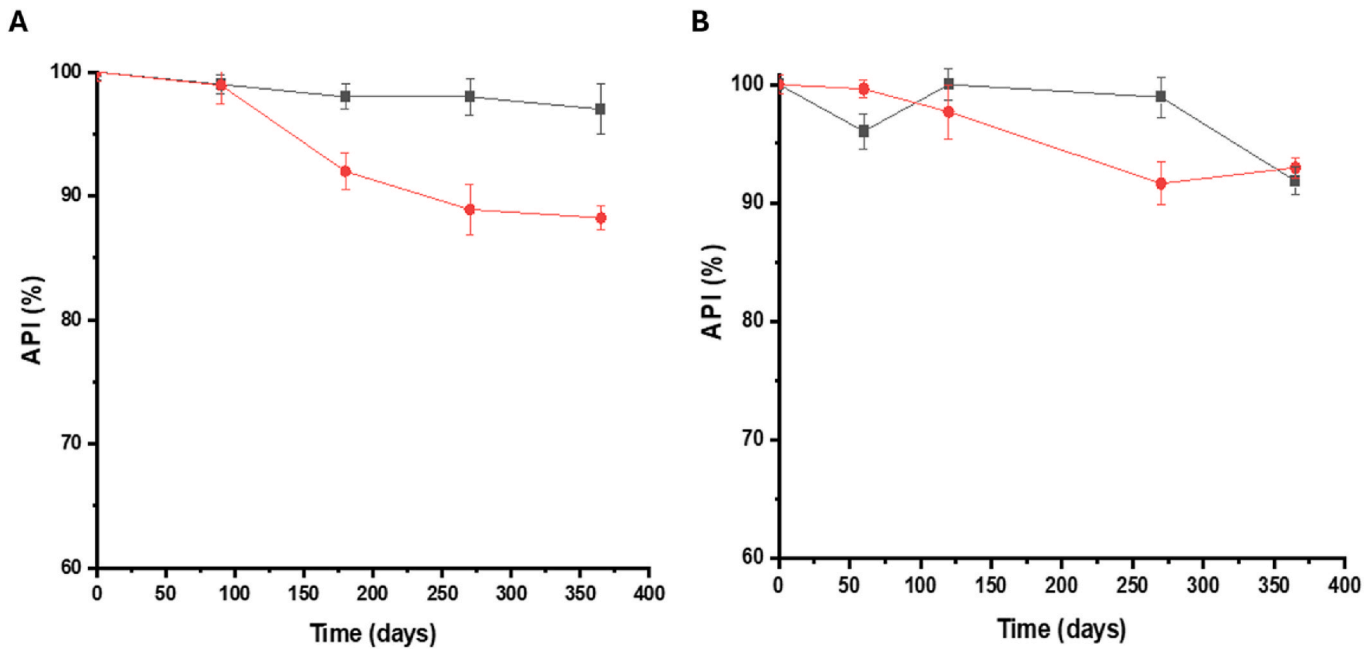

Fig. 7. AmB and vancomycin-loaded microparticles long-term chemical stability at different storage conditions. **a)** 5 ± 3 °C/10 % RH and **b)** 25 ± 2 °C/60 % RH ± 5 % RH. Key: (-●-) Vancomycin and (-■-) AmB.

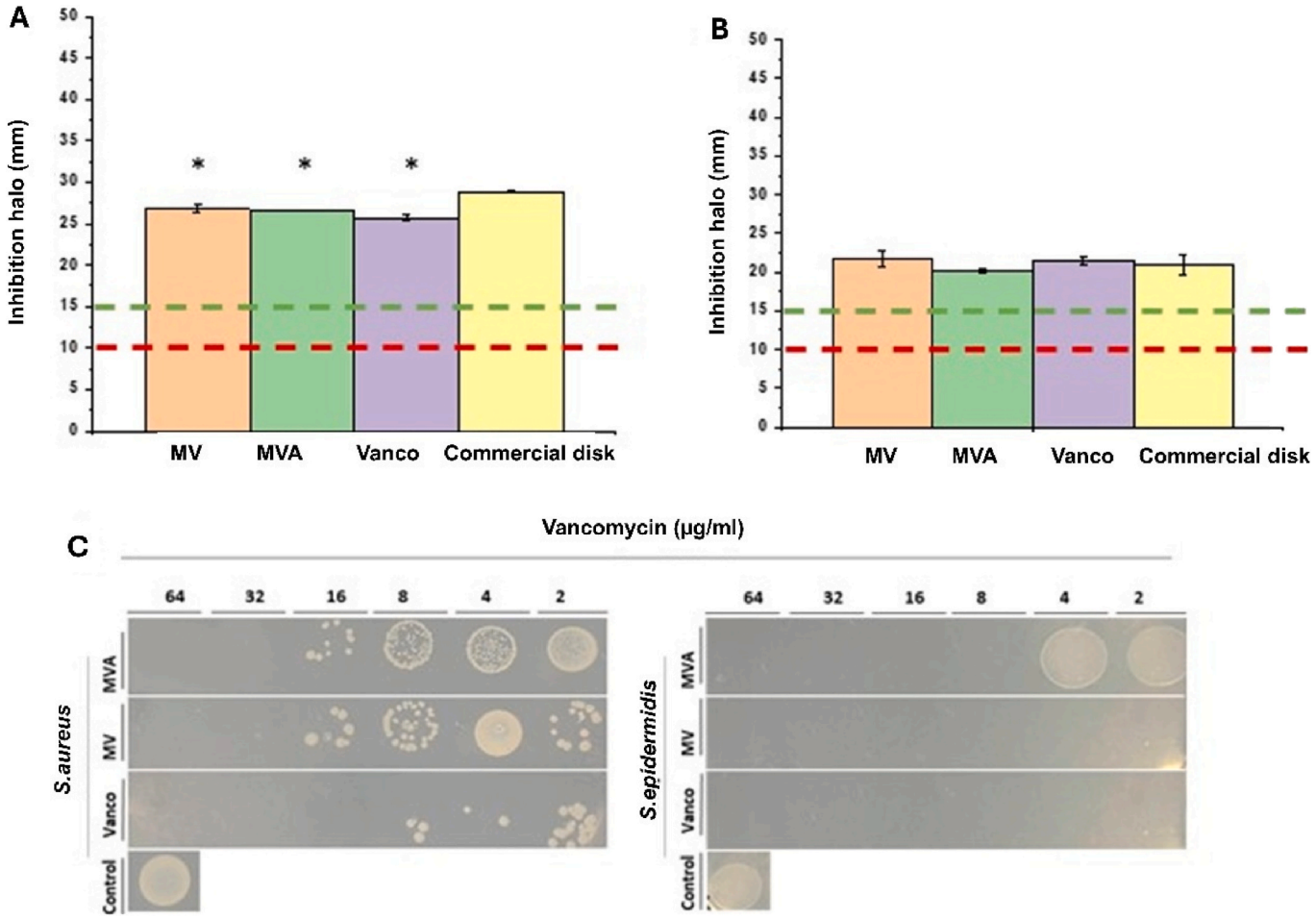

Fig. 8. ***In vitro*** **antibacterial efficacy assay against different species of** ***Staphylococcus*** **spp**. Key: (**MV**) Vancomycin-loaded microparticles; (**MVA**) AmB/Vancomycin-loaded microparticles and, (**Vanco**) Vancomycin dissolved in DMSO * Statistical differences ($p < 0.05$). Key: (**a**) *S. epidermidis,* (**b**) *S. aureus*. (**c**) Bacterial growth at different concentrations of vancomycin-loaded microparticles alone or in combination with AmB.

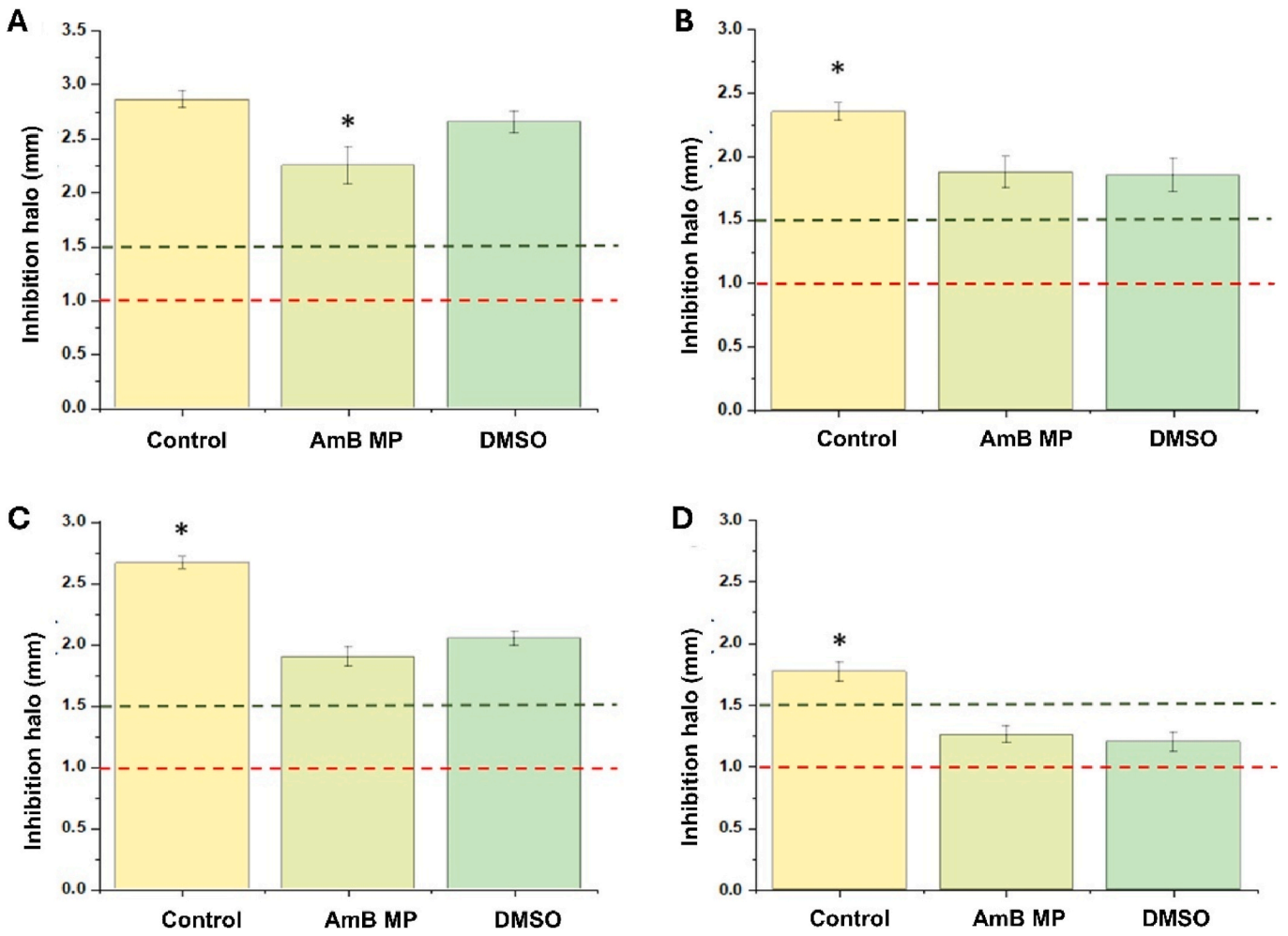

Fig. 9. ***In vitro*** **antifungal activity of AmB-loaded microparticles against different Candida spp.** *Key: (a) C. parapsilosis, (b) C.krusei, (c) C. albicans and (d) C. glabrata.* * Statistical differences ($p < 0.05$). The isolates were classified as susceptible (S) to AmB when the inhibition zone was ≥1.5 cm (green line), resistant (R) when it was ≤1 cm (red line) and intermediate (I) or susceptible-dose dependent when the inhibition zone was between 10- and 15-mm. MP, microparticle. (For interpretation of the references to colour in this figure legend, the reader is referred to the Web version of this article.)

RH conditions. This indicates that desiccated and refrigerated conditions are necessary to maintain the physicochemical stability of both AmB and vancomycin-loaded microparticles (Fig. 7). Predicted chemical stability from the Arrhenius equation agreed with the experimental long-term assessment.

3.7. Antibacterial in vitro assay

Antibacterial efficacy studies revealed an inhibition halo above 15 mm for all the formulations tested, including vancomycin-loaded microparticles, the AmB/vancomycin-loaded microparticles, and the drug dissolved in deionized water. This indicates that the drug can freely diffuse across the agar to elicit its antimicrobial effect. However, similarly to the antifungal activity, the sustained drug release profile led to a lower drug concentration in the media resulting in a lower efficacy compared to commercial disks of vancomycin when tested against *S. epidermidis*. For the *S. aureus,* no significant differences (*p*-value >0.05) were found between the microparticulate formulations and the Neo-Sensitabs™ discs. For *S. epidermidis,* the Minimum Inhibitory Concentration (MIC) was ≤2 μg/mL for vancomycin and vancomycin-loaded microparticles, while for the combined microparticles, the MIC was 8 μg/mL. For *S. aureus*, the MIC was 16 μg/mL for vancomycin dissolved in the agar medium and 32 μg/mL for vancomycin-loaded microparticles as well as the combined microparticles (Fig. 8).

3.8. Antifungal in vitro assay

All three strains (*C. albicans, C. glabrata, C. parapsilopsis*) were susceptible to AmB release from microparticles exhibiting a halo above 1.5 cm. However, the halo was below 1.5 cm but above 1.0 cm for *C. Krusei*, as it is well known that this species is more resistant to the effect of the drug. Despite the lower halo for *C. Krusei*, the halo was above 1.0 cm which indicates that the effect is dose-dependent and hence, greater AmB doses will be needed to eradicate a *C. krusei* infection (Fig. 9). Also, AmB release from microparticles showed a significant lower effect than AmB dissolved in DMSO. This can be linked to the slower release of AmB from the microparticles and hence, the lower drug concentration gradient achieved in the agar plate.

Regarding the absence or presence of colonies in Sabouraud agar plates, the Minimum Fungicidal Concentration (MFC) of AmB varied among different *Candida* spp, being the most susceptible species, *C. albicans* and *C. glabrata* (0.25 μg/mL) followed by *C. parapsilosis* (1 μg/mL), and *C. krusei* (2 μg/mL) to the AmB-loaded microparticles (Fig. 10). The efficacy of the combined AmB/Vancomycin was superior for *C. albicans* (MFC of 0.125 μg/mL) but lower for the rest of the *Candida* spp. tested. In all the cases, AmB dissolved in DMSO showed a greater activity considering that the sustained drug release from the microparticles reduced the available concentration of the drug at shorter times.

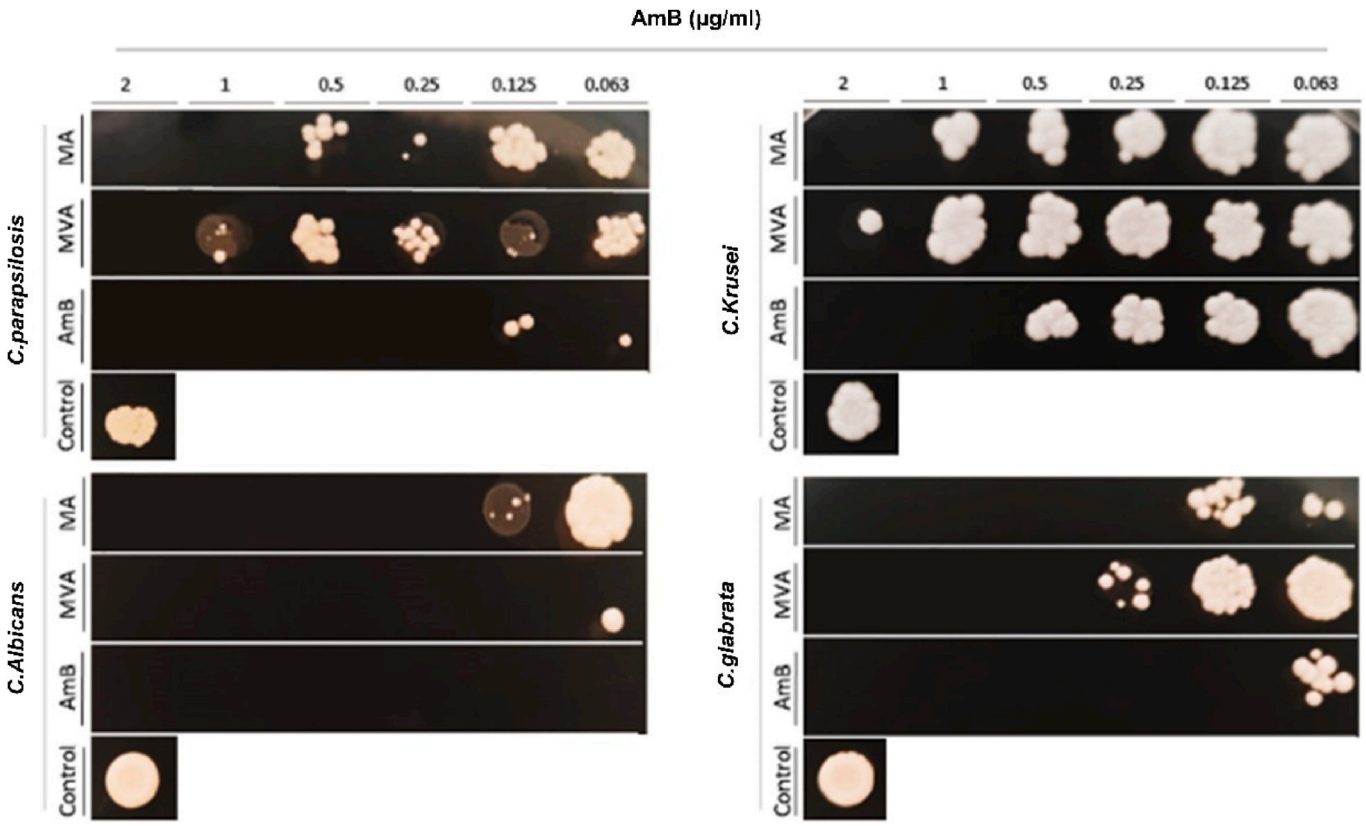

Fig. 10. Fungal growth at different concentrations of AmB or AmB/vancomycin microparticles. Key: (**MA**) AmB-loaded microparticles, (**MVA**) AmB/Vancomycin-loaded microparticles, and (**AmB**) Amphotericin B dissolved in DMSO.

3.9. Cytotoxicity assays

The cytotoxic effect of microparticles loaded with vancomycin, AmB, and vancomycin/AmB and the corresponding drugs in solution was evaluated on Saos-2, hFOB, and BJ cells for 24 h, 72 h, and 1 week by the MTT assay (Fig. 11). For Saos-2 cells, none of the treatments significantly affected the viability of the cells after the 24-h and 72-h incubation periods. However, after 1-week treatment, the results showed that AmB and the combination of AmB and vancomycin significantly reduced the viability of Saos-2 cells by around 40 %. For hFOB cells, after 24 h and 72 h of drug exposure, cell viability was significantly reduced below 40 % when treated with AmB and with AmB/vancomycin compared to the untreated cells. Moreover, after one week of treatment, a significant loss of viability was observed when the hFOB cells were treated with both AmB (0.9 % of cell viability) and AmB/vancomycin (5.9 %), but this cytotoxicity was also observed with the AmB-loaded microparticles (11.4 % viability) and the AmB/vancomycin-loaded microparticles (38.4 %). These results evidenced a significant cytoprotective effect when the drug was encapsulated within microparticles along with the AmB/vancomycin combination. Finally, for BJ cells, viability was significantly reduced over time with AmB and with AmB/vancomycin solutions but not when the drugs were encapsulated at all three treatment times. A significant cytoprotective effect was also observed with the microparticulate formulations as well as the AmB/vancomycin combination demonstrating a positive pharmacological interaction between AmB and vancomycin.

3.10. Evaluation of cell morphology by SEM

Fig. 12 shows the cell morphology of Saos-2, hFOB, and BJ cells after 7 days of exposition to different treatments. In these three cell lines, it is worth noting that the exposition to free AmB or the combination of AmB/vancomycin significantly affects cell morphology, as well as the areas of growing, were sparsely populated with cells. The drug encapsulation in microparticles exerted a protective cell effect, especially from AmB and the combination of both drugs.

4. Discussion

The rationale of this work for combining antifungal and antibacterial agents in the treatment of PJIs is primarily driven by the complex nature of polymicrobial infections, which often involve both bacterial and fungal pathogens. This dual approach aims to address the multifaceted challenges posed by biofilm formation, microbial resistance, and the presence of mixed infections, thereby improving treatment outcomes and reducing morbidity and mortality associated with PJIs [51].

Localized antibiotic administration has been explored as a prophylactic strategy in primary joint replacement, with delivery as a powder or solution achieving high intraoperative concentrations. However, rapid post-surgical decline often results in subtherapeutic levels, limiting its clinical efficacy [52]. To sustain high local antibiotic concentrations while minimizing systemic exposure, intra-articular catheters or drug carriers have been proposed to enhance pharmacokinetics and antimicrobial efficacy [53]. For this reason, bioactive materials, such as antibiotic hydrogels and microparticles, are being explored for their potential to prevent and treat PJIs. These materials can enhance the delivery and efficacy of antifungal and antibacterial agents [54,55].

Antifungal agents such as AmB, voriconazole, and fluconazole have been used in acrylic bone cement to treat fungal PJIs. Some cases have combined these antifungals with antibiotics to address coexisting bacterial infections, although data on clinical efficacy is limited and further research is needed [56]. Calcium sulphate beads have been used successfully in treating atypical bacterial and fungal super-infections in PJIs [57]. However, its clinical application is limited by risks of wound

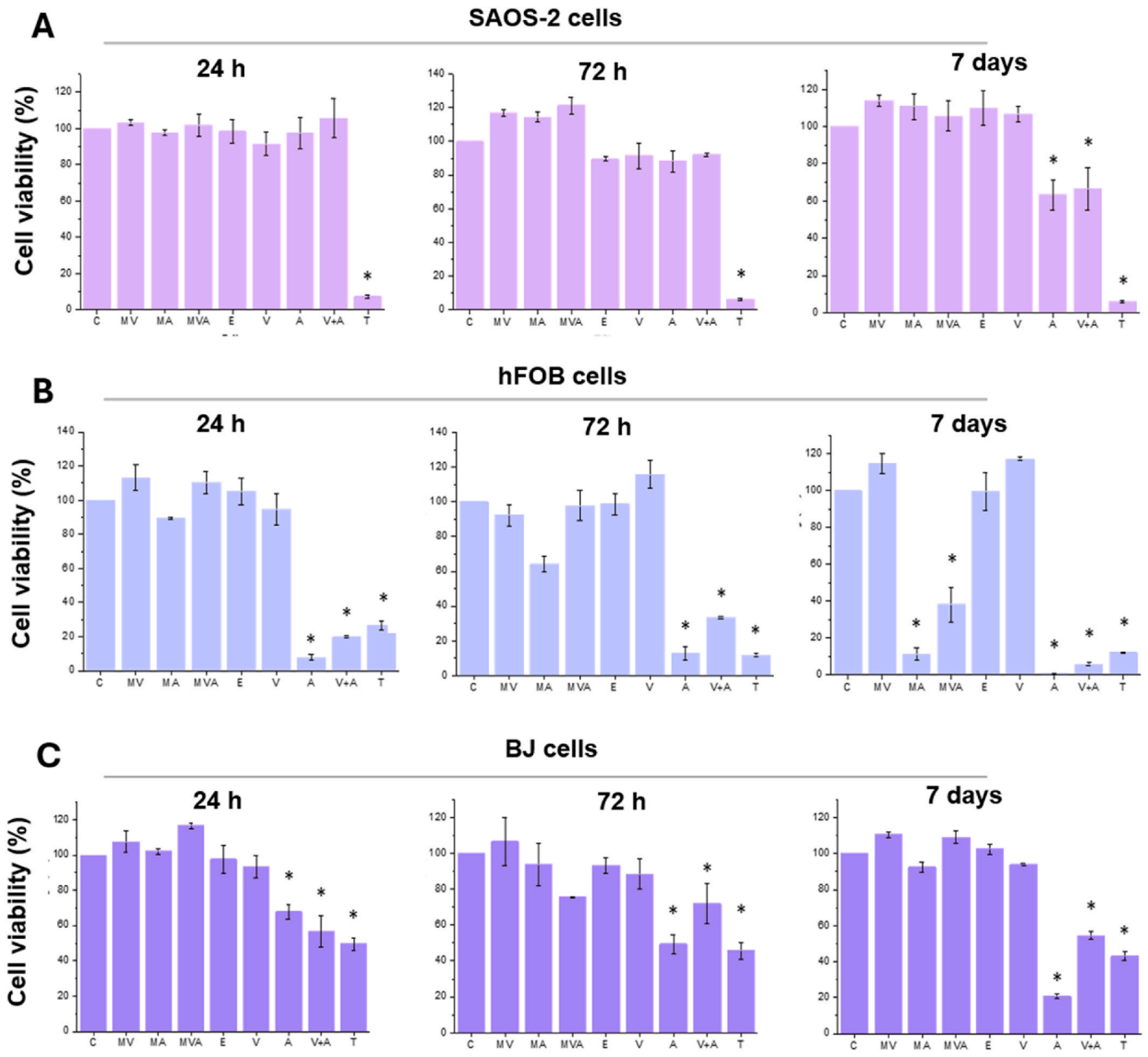

Fig. 11. Effect on a) Saos-2, b) hFOB and c) BJ cell viability. Cells were treated with microparticles loaded with vancomycin, AmB and AmB/vancomycin, as well as the drugs as control for 24 h, 72 h and 7 days. Cytotoxicity was analyzed by MTT assay. Key: (**C**) Control; (**MV**) Vancomycin-loaded microparticles; (**MA**) AmB-loaded microparticles; (**MVA**) AmB/vancomycin-loaded microparticles; (**E**) Blank spray dried microparticles; (**V**) Free vancomycin; (**A**) Free AmB; (**V + A**) Free vancomycin and AmB; (**T**) Triton.

leakage and hypercalcemia [58]. In other hands, bacteriophages represent a promising alternative due to their high specificity and lack of mammalian toxicity; nonetheless, their applicability to PJIs remains constrained by the need for extensive phage collections [59]. Hydrogels offer tuneable drug release, high antimicrobial compatibility, and adaptability to patient-specific needs, yet their clinical translation remains largely unexplored [60,61]. In our study, we demonstrate the potential of bioadhesive microparticulate hydrogels as a dual prophylactic and therapeutic strategy for PJIs. Our formulation enables controlled and sustained antibiotic release while maximizing local drug concentrations, overcoming limitations associated with conventional delivery systems. These findings highlight microparticulate hydrogels as a promising alternative for PJI management, warranting further clinical investigation.

Biofilms formed by *Staphylococci* in PJIs exhibit significantly higher resistance to antibiotics compared to planktonic bacteria. For instance, biofilms can be over 8000 times more resistant to antimicrobial agents, which complicates treatment and increases the risk of infection recurrence [62]. Similarly, biofilm formation by *S. lugdunensis* was linked to relapsing PJIs, underscoring the clinical impact of biofilms [63]. Incorporating biofilm susceptibility testing, such as determining the minimum biofilm eradication concentration (MBEC), can guide more effective antibiotic regimens. This approach is being evaluated in clinical trials to improve treatment outcomes by tailoring therapies to the biofilm growth mode of bacteria [64]. Research is exploring new treatment modalities, including the use of nanoparticles, lytic bacteriophages, and photodynamic therapy, to target biofilm-related infections. These strategies aim to enhance the effectiveness of conventional antibiotics and offer alternative solutions for managing PJIs [55]. Our bioadhesive microparticulate hydrogel system loaded

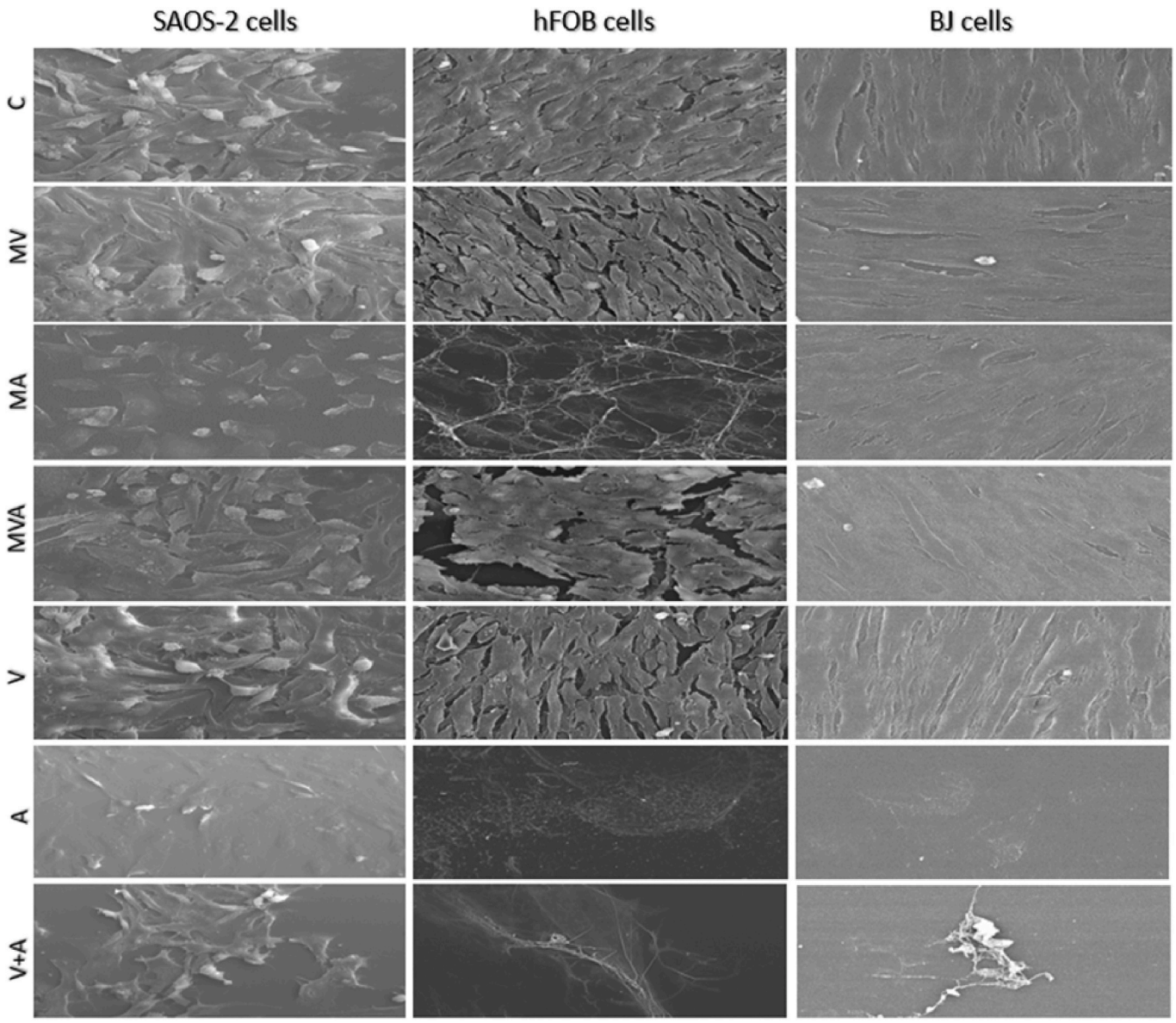

Fig. 12. SEM images (magnification ×500) of Saos-2 cells, hFOB cells, and BJ cells treated with microparticles loaded with vancomycin, AmB, and vancomycin/AmB and the corresponding drugs for 1 week.

with AmB and vancomycin represents a novel approach by simultaneously addressing bacterial and fungal infections. Although further *in vivo* studies are required, these initial findings suggest a promising direction for managing biofilm-associated PJIs.

Successful treatment of PJIs involving both methicillin-resistant *Staphylococcus aureus* (MRSA) and *Candida albicans* has been documented, utilizing a combination of local and systemic antifungal and antibacterial therapies. These cases highlight the importance of tailored treatment plans and the potential for DAIR (debridement, antibiotics, and implant retention) in managing complex infections [65]. Our findings align with this perspective, as the bioadhesive microparticulate hydrogel demonstrated significant antimicrobial activity against both *S. aureus* and *C. albicans*. Furthermore, the sustained drug release profile maintained effective local antibiotic concentrations beyond 72 h, addressing the limitations of conventional antibiotic administration.

Ongoing clinical trials are evaluating novel antibiotic regimens and their impact on PJI treatment outcomes, particularly for infections caused by *S. aureus* [66]. Our study provides evidence supporting the use of microparticulate hydrogels as an innovative delivery system that enhances antibiotic retention at the infection site while minimizing systemic exposure. Given the challenges posed by biofilm-associated infections, the ability of our formulation to prolong drug activity and inhibit microbial colonization suggests its potential as both a prophylactic and therapeutic strategy. In addition, our cytotoxicity assays indicate >90 % cell viability, suggesting that the hydrogel does not negatively affect mammalian cells. Additionally, our formulation does not induce haemolysis, supporting its safety for *in vivo* application. While hydrogels are generally considered favourable for osseointegration, further mechanical wear studies are needed to assess their long-term stability.

Following this premise, we have developed a hyaluronic-based hydrogel that incorporates antimicrobial drugs in microparticulate systems to prolong drug release for one week. The sustained release provided by microparticles resulted in excellent biocompatibility with a significant reduction in haemotoxicity, especially with AmB which is highly haemolytic, but also no signs of toxicity were observed in osteoblasts and fibroblasts. Drug releases were performed mimicking the joint cavity with limited access to physiological fluids. Even with the

slower release, the resulting antimicrobial concentration in aqueous media exhibited good antimicrobial activity, which indicated that the release rate was suitable to elicit a pharmacological effect at the joint space. It is worth noting that the combination of AmB and vancomycin within the same microparticulate carrier has shown to be a promising approach for PJIs targeting both bacterial and fungal infections with complementary hydrophilicity, amphiphilic for AmB and hydrophilic for vancomycin. This makes it feasible to prolong the release of vancomycin while enhancing the release of AmB. Even though, further *in vivo* studies need to be performed to confirm the pharmacological-toxicological profile, in this work we have demonstrated for the first time a novel approach to treat and prevent PJIs based on bioadhesive microparticulate hydrogels.

5. Conclusions

The microparticles showed a sustained release profile marked by a burst release followed by a controlled release until 7 days. The excipients were carefully selected, and drug encapsulation resulted in higher biocompatibility against mammalian cells (RBCs, osteoblasts, and fibroblasts) and excellent antimicrobial efficacy against bacteria and fungi. The formulation showed optimal adhesion profile to the prosthesis in less than 5 min avoiding extending the surgical procedure. These results show this microparticulate formulation could be a novel and promising approach for the treatment of PJIs. However, further *in vivo* studies need to be performed to confirm the pharmacological-toxicological profile.

CRediT authorship contribution statement

F.C. Luciano: Writing – original draft, Methodology, Investigation, Formal analysis, Data curation, Conceptualization. **I. Yuste:** Writing – review & editing, Methodology, Investigation, Formal analysis, Data curation. **P. Sanz-Ruiz:** Writing – review & editing, Supervision, Resources, Methodology, Funding acquisition, Conceptualization. **A. Ribed-Sánchez:** Writing – review & editing, Resources, Methodology, Funding acquisition, Conceptualization. **M.P. Ballesteros:** Writing – review & editing, Supervision, Resources, Project administration, Funding acquisition, Conceptualization. **C. Rodríguez:** Supervision, Resources, Methodology. **B.J. Anaya:** Writing – review & editing, Methodology, Formal analysis. **M. Tiboni:** Writing – review & editing, Methodology, Formal analysis, Data curation. **G. Maurizzi:** Methodology, Formal analysis, Data curation. **L. Casettari:** Writing – review & editing, Supervision, Resources, Project administration, Methodology, Funding acquisition. **E. González-Burgos:** Writing – review & editing, Supervision, Resources, Project administration, Methodology, Funding acquisition, Formal analysis. **D.R. Serrano:** Writing – review & editing, Supervision, Resources, Project administration, Methodology, Funding acquisition, Formal analysis, Data curation, Conceptualization.

Declaration of competing interest

The authors declare that they have no known competing financial interests or personal relationships that could have appeared to influence the work reported in this paper.

Acknowledgments

This study was partially supported by the Complutense University of Madrid Research Group 971089 (Innovation in Pharmacology, Nanotechnology, and Personalized Medicine by 3D Printing). Dolores Serrano acknowledges the support received from ESCMID 2021 research grants (16306). This study has been also funded by the Spanish Ministry of Science and Innovation – Agencia Estatal de Investigación (award PID2021-126310OA-I00) to Dolores Serrano.

Appendix A. Supplementary data

Supplementary data to this article can be found online at https://doi.org/10.1016/j.jddst.2025.107001.

Data availability

Data will be made available on request.

References

[1] S.K. Kunutsor, et al., Patient-related risk factors for periprosthetic joint infection after total joint arthroplasty: a systematic review and meta-analysis, PLoS One 11 (3) (2016) e0150866.
[2] J. Parvizi, et al., Periprosthetic joint infection: the economic impact of methicillin-resistant infections, J. Arthroplast. 25 (6) (2010) 103–107.
[3] M.M. Martínez-Suárez, J.C.A. L, D. Alonso-Álvarez, A.J. López-Díaz, A. Fernández-Somoano, A. Tardón-García, Tasas de infección de herida quirúrgica en artroplastia de cadera, Journal of Healthcare Quality Research 33 (4) (2018) 219–224.
[4] M. Franco Arenaz, Epidemiología De La Infección De Prótesis Articular En España En La Última Década. Análisis De La Evolución De La Etiologia En El Tiempo, Universidad Autonoma de Barcelona Barcelona, 2017.
[5] W.T.A. Zimmerli, P.E. Ochsner, Prosthetic-joint infections, N. Engl. J. Med. (351) (2004) 1645–1654.
[6] Z.R. Sambri A, M. Fiore, M. Bortoli, A. Paolucci, M. Filippini, E. Zamparini, S. Tedeschi, P. Viale, M. De Paolis, Epidemiology of fungal periprosthetic joint infection: a systematic review of the literature 11 (1) (2022) 84, https://doi.org/10.3390/microorganisms11010084.
[7] L.F. Chisari E, J. Fei, J. Parvizi, Fungal periprosthetic joint infection: rare but challenging problem, Chin. J. Traumatol. (Engl. Ed.) 25 (2) (2022) 63–66.
[8] M. Rozis, D.S. Evangelopoulos, S.G. Pneumaticos, Orthopedic implant-related biofilm pathophysiology: a review of the literature, Cureus 13 (6) (2021) e15634.
[9] R.S. Murdoch Dr, V.G. Fowler Jr., et al., Infection of orthopedic prostheses after Staphylococcus aureus bacteremia, Clin. Infect. Dis. (32) (2001) 647–649.
[10] P.B.O. Zakovicova, A. Trampuz, Periprosthetic joint infection: current concepts and outlook, EFORT Open Rev. 4 (7) (2019) 482–494.
[11] C.E. Gross, et al., Fungal periprosthetic joint infection: a review of demographics and management, J. Arthroplast. 36 (5) (2021) 1758–1764.
[12] E. Chisari, et al., Fungal periprosthetic joint infection: rare but challenging problem, Chin. J. Traumatol. (Engl. Ed.) 25 (2) (2022) 63–66.
[13] T.S. Brown, et al., Periprosthetic joint infection with fungal pathogens, J. Arthroplast. 33 (8) (2018) 2605–2612.
[14] R. Figa, et al., Periprosthetic joint infection by propionibacterium acnes: clinical differences between monomicrobial versus polymicrobial infection, Anaerobe 44 (2017) 143–149.
[15] L. Flurin, K.E. Greenwood-Quaintance, R. Patel, Microbiology of polymicrobial prosthetic joint infection, Diagn. Microbiol. Infect. Dis. 94 (3) (2019) 255–259.
[16] M. McNally, et al., What IS the best surgical option for periprosthetic joint infection (PJI) due to CANDIDA species?, in: Orthopaedic Proceedings Bone & Joint, 2024.
[17] G. Shang, et al., The heavy burden and treatment challenges of fungal periprosthetic joint infection: a systematic review of 489 joints, BMC Muscoskelet. Disord. 25 (1) (2024) 648.
[18] L. Zhong, et al., Incidence, clinical characteristics, risk factors and outcomes of patients with mixed candida/Bacterial bloodstream infections: a retrospective study, Ann. Clin. Microbiol. Antimicrob. 21 (1) (2022) 45.
[19] Y. Luo, et al., Targeting Candida albicans in dual-species biofilms with antifungal treatment reduces Staphylococcus aureus and MRSA in vitro, PLoS One 16 (4) (2021) e0249547.
[20] P. Joshi, P. Danu, D. Gajjar, Candida: an important partner in polymicrobial colonization on indwelling medical devices, Med. Mycol. 60 (S1) (2022) 91.
[21] C. Belgiovine, et al., Interaction of bacteria, immune cells, and surface topography in periprosthetic joint infections, Int. J. Mol. Sci. 24 (10) (2023) 9028.
[22] N.S. Shabana, et al., The clinical outcome of early periprosthetic joint infections caused by Staphylococcus epidermidis and managed by surgical debridement in an era of increasing resistance, Antibiotics 12 (1) (2022) 40.
[23] Y. Chang, et al., Pathogenic bacteria characteristics and drug resistance in acute, delayed, and chronic periprosthetic joint infection: a retrospective analysis of 202 patients, Int. Wound J. 20 (8) (2023) 3315–3323.
[24] M. Marquez-Gomez, et al., Does a specific sequential combination of antiseptic solutions for chemical debridement in periprosthetic joint infection improve outcomes vs. solution alone? An in vivo study, Antibiotics (Basel) 13 (12) (2024).
[25] C. Li, N. Renz, A. Trampuz, Management of periprosthetic joint infection, Hip Pelvis 30 (3) (2018) 138–146.
[26] P. Izakovicova, O. Borens, A. Trampuz, Periprosthetic joint infection: current concepts and outlook, EFORT Open Rev. 4 (7) (2019) 482–494.
[27] C. Xu, et al., Is treatment of periprosthetic joint infection improving over time? J. Arthroplast. 35 (6) (2020) 1696–1702e1.
[28] K.M. Natsuhara, et al., Mortality during total hip periprosthetic joint infection, J. Arthroplast. 34 (7S) (2019) S337–S342.
[29] J. Lu, et al., Infection after total knee arthroplasty and its gold standard surgical treatment: spacers used in two-stage revision arthroplasty, Intractable Rare Dis Res 6 (4) (2017) 256–261.

[30] M. Taha, et al., New innovations in the treatment of PJI and biofilms-clinical and preclinical topics, Curr Rev Musculoskelet Med 11 (3) (2018) 380–388.
[31] M.T. Houdek, et al., Elution of high dose amphotericin B deoxycholate from polymethylmethacrylate, J. Arthroplast. 30 (12) (2015) 2308–2310.
[32] I.S. Ferreira, et al., Activity of daptomycin- and vancomycin-loaded poly-epsilon-caprolactone microparticles against mature staphylococcal biofilms, Int. J. Nanomed. 10 (2015) 4351–4366.
[33] I. Soares, et al., Drug delivery from PCL/chitosan multilayer coatings for metallic implants, ACS Omega 7 (27) (2022) 23096–23106.
[34] R. Espada, et al., HPLC assay for determination of amphotericin B in biological samples, Biomed. Chromatogr. 22 (4) (2008) 402–407.
[35] D.R. Serrano, et al., Hemolytic and pharmacokinetic studies of liposomal and particulate amphotericin B formulations, Int. J. Pharm. 447 (1–2) (2013) 38–46.
[36] M.J. de Jesús Valle, F.G. López, A.S. Navarro, Development and validation of an HPLC method for vancomycin and its application to a pharmacokinetic study, J. Pharmaceut. Biomed. Anal. 48 (3) (2008) 835–839.
[37] L.A. Serrano Dr, M.A. Dea-Ayuela, P.E. Bilbao-Ramos, N.L. Garrett, J. Moger, J. Guarro, J. Capilla, M.P. Ballesteros, A.G. Schätzlein, F. Bolás, J.J. Torrado, I. F. Uchegbu, Oral particle uptake and organ targeting drives the activity of amphotericin B nanoparticles, Mol. Pharm. 12 (2) (2015) 420–431.
[38] M.D.N.M. Sánchez-Somolinos, A. Benjumea, M. Tormo, J. Matas, J. Vaquero, P. Muñoz, P. Sanz-Ruíz, M. Guembe, Determination of the elution capacity of dalbavancin in bone cements: new alternative for the treatment of biofilm-related peri-prosthetic joint infections based on an in vitro study, Antibiotics (Basel) 11 (10) (2022) 1300.
[39] H.K. Ruiz, et al., New amphotericin B-gamma cyclodextrin formulation for topical use with synergistic activity against diverse fungal species and leishmania spp, Int. J. Pharm. 473 (1–2) (2014) 148–157.
[40] R. Fernandez-Garcia, et al., Self-assembling, supramolecular chemistry and pharmacology of amphotericin B: poly-Aggregates, oligomers and monomers, J. Control. Release 341 (2022) 716–732.
[41] B.J. Anaya, et al., Engineering of 3D printed personalized polypills for the treatment of the metabolic syndrome, Int. J. Pharm. 642 (2023) 123194.
[42] I. Pineros, et al., Analgesic and anti-inflammatory controlled-released injectable microemulsion: pseudo-Ternary phase diagrams, in vitro, ex vivo and in vivo evaluation, Eur. J. Pharm. Sci. 101 (2017) 220–227.
[43] R. Fernandez-Garcia, et al., Ultradeformable lipid vesicles localize amphotericin B in the dermis for the treatment of infectious skin diseases, ACS Infect. Dis. 6 (10) (2020) 2647–2660.
[44] D.R. Serrano, et al., Designing fast-dissolving orodispersible films of amphotericin B for oropharyngeal candidiasis, Pharmaceutics 11 (8) (2019).
[45] D.R. Serrano, et al., Optimising the in vitro and in vivo performance of oral cocrystal formulations via spray coating, Eur. J. Pharm. Biopharm. 124 (2018) 13–27.
[46] K.C. Waterman, R.C. Adami, Accelerated aging: prediction of chemical stability of pharmaceuticals, Int. J. Pharm. 293 (1–2) (2005) 101–125.
[47] M. Rolon, et al., Solid nanomedicines of nifurtimox and benznidazole for the oral treatment of chagas disease, Pharmaceutics 14 (9) (2022).
[48] B. Herigstad, M. Hamilton, J. Heersink, How to optimize the drop plate method for enumerating bacteria, J. Microbiol. Methods 44 (2) (2001) 121–129.
[49] D.R. Serrano, et al., A novel formulation of solubilised amphotericin B designed for ophthalmic use, Int. J. Pharm. 437 (1–2) (2012) 80–82.
[50] J.J. Torrado, D.R. Serrano, I.F. Uchegbu, The oral delivery of amphotericin B, Ther. Deliv. 4 (1) (2013) 9–12.
[51] J.A.M.-D. Pablo Sanz-Ruiz, Manuel Villanueva-Martínez, Alex Dos Santos-Vaquinha Blanco, Vaquero Javier, Is dual antibiotic-loaded bone cement more effective and cost-efficient than a single antibiotic-loaded bone cement to reduce the risk of prosthetic joint infection in aseptic revision knee arthroplasty? J. Arthroplast. 34 (12) (2020) 3724–3729.
[52] J.D. Johnson, et al., Serum and wound vancomycin levels after intrawound administration in primary total joint arthroplasty, J. Arthroplast. 32 (3) (2017) 924–928.
[53] W. Steadman, et al., Local antibiotic delivery options in prosthetic joint infection, Antibiotics (Basel) 12 (4) (2023).
[54] H. Xie, Y. Liu, H. An, Recent advances in prevention, detection and treatment in prosthetic joint infections of bioactive materials. Front Bioeng Biotechnol 10 (2022) 1–16.
[55] M. Taha, et al., New innovations in the treatment of PJI and Biofilms—Clinical and preclinical topics, Current reviews in musculoskeletal medicine 11 (2018) 380–388.
[56] K. Anagnostakos, S.L. Becker, I. Sahan, Antifungal-loaded acrylic bone cement in the treatment of periprosthetic hip and knee joint infections: a review, Antibiotics 11 (7) (2022) 879.
[57] A.P. Kurmis, Eradicating fungal periprosthetic TKA "super-infection": review of the contemporary literature and consideration of antibiotic-impregnated dissolving calcium sulfate beads as a novel PJI treatment adjunct, Arthroplasty Today 8 (2021) 163–170.
[58] M.Y. Tarar, et al., Wound leakage with the use of calcium sulphate beads in prosthetic joint surgeries: a systematic review, Cureus 13 (11) (2021) e19650.
[59] T. Ferry, et al., Past and future of phage therapy and phage-derived proteins in patients with bone and joint infection, Viruses 13 (12) (2021).
[60] I. Yuste, et al., Engineering 3D-Printed advanced healthcare materials for periprosthetic joint infections, Antibiotics (Basel) 12 (8) (2023).
[61] D.R. Serrano, et al., 3D printing technologies in personalized medicine, nanomedicines, and biopharmaceuticals, Pharmaceutics 15 (2) (2023).
[62] K.S. Malchau, et al., Biofilm properties in relation to treatment outcome in patients with first-time periprosthetic hip or knee joint infection, Journal of orthopaedic translation 30 (2021) 31–40.
[63] M. Hagstrand Aldman, O. Thompson, L.I. Påhlman, Biofilm formation is associated with poor outcome in prosthetic joint infections caused by Staphylococcus lugdunensis, Infect. Dis. (Lond.) 55 (5) (2023) 328–332.
[64] J.A. Tillander, et al., Treatment of periprosthetic joint infections guided by minimum biofilm eradication concentration (MBEC) in addition to minimum inhibitory concentration (MIC): protocol for a prospective randomised clinical trial, BMJ Open 12 (9) (2022) e058168.
[65] Y. Xiang, Y.-Y. Xuan, G. Li, Successful treatment for acute prosthetic joint infection due to MRSA and candida albicans: a case report and literature review, Therapeut. Clin. Risk Manag. (2018) 1133–1139.
[66] Á. Auñón, et al., Does a new antibiotic scheme improve the outcome of staphylococcus aureus-caused acute prosthetic joint infections (PJI) treated with debridement, antibiotics and implant retention (DAIR)? Antibiotics 11 (7) (2022) 922.